UNIVERSITÀ DEGLI STUDI DI GENOVA

FACOLTÀ DI INGEGNERIA

Tesi di Laurea Specialistica
in

INGEGNERIA MECCANICA

Local Stability Analysis of a Coaxial Jet at low Reynolds Number

Candidato:
Giacomo Gallino

Relatore:
Chiar.mo Prof.
Alessandro Bottaro

Relatore:
Prof.
François Gallaire

Anno accademico 2011/2012

Riassunto

La formazione di gocce in getti a bassi numeri di Reynolds è un fenomeno di grande interesse dal punto di vista ingegneristico, essendo molte le sue possibili applicazioni in diversi processi industriali. Solo per nominarne alcune: stampanti a getto d'inchiostro, processi di emulsificazione e estrusione di polimeri. Motivati da queste possibili applicazioni, abbiamo studiato la stabilità di getti coassiali in microcanali. La configurazione fisica osservata è una variante del classico problema di Rayleigh-Plateau, dove però imponiamo confinamento del getto. Da studi precedenti è stata osservata sperimentalmente la transizione tra situazioni dove il flusso forma un getto (regime di jetting) o dove forma delle gocce (regime di dripping). Il verificarsi di questi due regimi è stato giustificato dal tipo di instabilità presente nel flusso che può essere convettiva o assoluta. Eseguendo analisi di stabilità locale per diverse coordinate assiali del flusso, abbiamo studiato il flusso nella regione in cui si sviluppa e abbiamo proposto un'interpretazione dei meccanismi che regolano la transizione tra regime di jetting e regime di dripping.

Abstract

Droplets formation in jets at low Reynolds number is a phenomenon of great engineering interest because of its applicability in industrial processes. Just to name a few: ink-jet printing, emulsification process and polymer extrusion. Motivated by these possible applications, we study the stability of coaxial biphasic jets in micro-channels. The physical configuration observed is a variant of the classical Rayleigh-Plateau problem, where we impose wall confinement. In previous studies it has been observed experimentally the transition between situations where the flow takes the forms of a jet (jetting regime) or where it forms droplets (dripping regime). These two regimes are explained with the flow being convectively unstable or absolutely unstable. Performing local stability analysis for various axial coordinate of the flow, we analyze the developing region and we propose an interpretation of the mechanisms that rule the transition between jetting and dripping regime.

Acknowledgments

I would like to express my gratitude to all the people who have contributed to the realization of this project. Especially I want to thank Alessandro Bottaro and François Gallaire, they have supervised my work and really helped me in this first experience in the research world. My gratitude is also for the members of the lab (LFMI-EPFL) in which I've worked in these months spent in Switzerland: Laura Augello for her patience and availability; Mathias Nagel for his competence about the boundary element method; Francesco Viola and Marc-Antoine Habisreutinger for their knowledge and for the wonderful week-ends spent skiing in the Swiss Alps; Edouard Boujo who taught me not only about FreeFem but also about climbing; Cristobal Arratia, Pierre-Thomas Brun, Vladislav Lugo and Yoan Marchand for their friendship that made me feel like at home during these months.

Preface

The work presented in this project is the result of a collaboration between the Laboratory of Fluid Mechanics and Instabilities (LFMI), EPFL, Lausanne (Switzerland), and the Department of Civil, Chemical and Environmental Engineering, University of Genova. The work has been carried out under the supervision of Alessandro Bottaro (UNIGE) and François Gallaire, head director of the LFMI-EPFL. The whole active has been realized, between September 2012 and February 2013 at the EPFL, as part of a wider project focused on the stability analysis of flows at low Reynolds number; this is done in order to be able to predict droplets formation in micro-channels.

In the first stage of the project I have written a MATLAB code, using the boundary element method, to simulate numerically the physical phenomenon. In the second stage I have adapted an in-house MATLAB code (from LFMI) to my problem. These two tools make possible to perform stability analysis on the flow studied. The numerical tool that I have developed in the frame of the project will be used to carry on studies on the stability of flows characterized from low Reynolds number and axisymmetric configurations.

Contents

Introduction

Stability of jets is of great engineering interest since the work of Rayleigh [1] and Plateau [2] about jets instability; in fact it is very common to find this kind of phenomena in many industrial applications from energy generation to chemical processes. The jets analyzed in this project model those found in applications, like ink-jet printers (figure 1). Ink-printers are very interesting to study because the same technology could also be used to manufacture high technology products, for example polymer extrusion of use in the microchip industry (figure 2). Other applications vary from food to biomedical industry, for example in the second one it could be important to know if a drug injected in vein forms droplets before or after it touches the organ to which it is destined.

The jets present in the applications described above belong to a particular class: coaxial confined jets at low Reynolds number. The configuration of the system we will study is composed of a microchannel (the size of the radius of the channel is about $10^{-4}m$) where two immiscible fluids touch each other (cf. figure 2.2); the two fluids can not mix because of surface tension. From experimental and analytical studies this configuration has always yielded an instability that leads to droplets formation, as we can see in figure 4. Sometimes the droplet is formed just outside the inlet (dripping) and sometimes we can identify a jet after which the droplet is formed (jetting). In [5] the stability of the fully developed flow (for which an analytical solution exists under lubrication theory simplification) has been studied; the flow is always locally unstable, the criterion to predict dripping

Figure 1: Ink-jets, experimental study by Steve Hoath in [3].

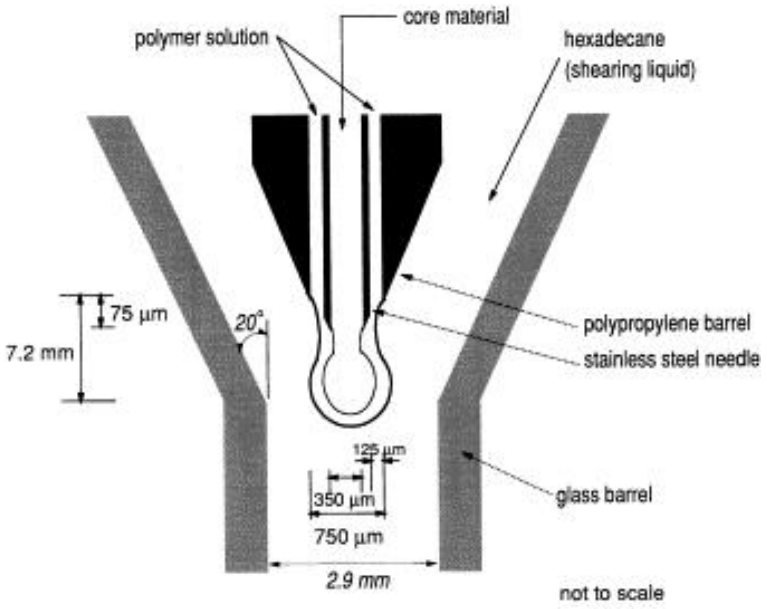

Figure 2: Polymer extrusion presented in [4], the flow of hexadecane push the polymer at the tip of the nozzle that detaching forms the droplets.

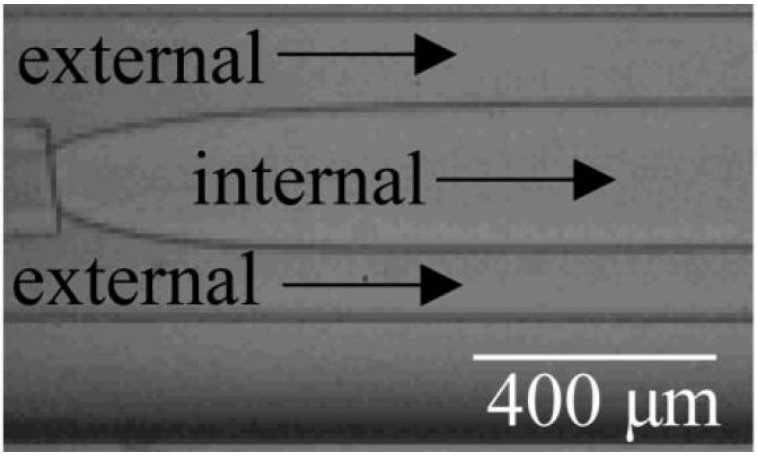

Figure 3: Flow configuration, experimental study presented in [5].

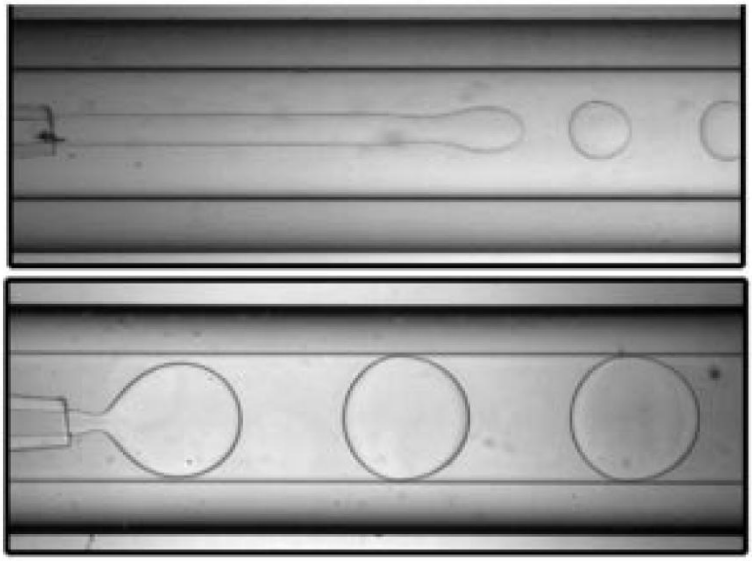

Figure 4: Two different regimes of droplets formation, jetting and dripping, experimental study presented in [5].

or jetting regime is to look if the instability is absolute or convective. If it is absolute the instability is strong enough for the disturbance to move upstream and the dripping regime is thus formed; otherwise the instability is washed away from the flow and the jetting regime is reached. In [5] a qualitatively good transition region between dripping and jetting regime is found, although in some cases the difference between the experimental results and the analytical solutions seems quite significant.

In this project the main idea is to perform local stability analysis in the developing region, where we believe important mechanisms regarding the droplets formation are localized. In this way, not applying lubrication theory, we hope to have a deeper understanding of the phenomenon and to find better agreement with the experimental results.

What is done, more in detail, is to find a stable configuration of the system; since this is not physically possible, we will force the system to be stable. This stable configuration is found numerically with a code written in MATLAB in the frame of this work, using the boundary elements method. How this is done will be explained in chapter 1. Once the stable configuration is reached we perform local stability analysis in the region close to the inlet. In practice we add small perturbations at the stable solution and look if the configuration remains stable or not. The method to do this will be explained in chapter 2. From the results in the developing region we should capture effects which are not taken into account when looking only at the developed region. For example, we could find that a flow that has a convective mode in the developed region is actually characterized from an absolute instability in the developing region, this eventually leading to a dripping regime. On the other hand a convective mode in the developing region could wash away an absolute mode coming from the developed region, yielding the jetting regime.

Chapter 1

Base flow calculations

1.1 The base

To perform the stability analysis we first need a stationary configuration of the system, the base flow is in fact a so called fixed point, a base configuration that does not change if not perturbed. In our case we have a coaxial jet and we expect droplets formation when the interface between the fluids touches the axis. Droplets formation is thought to be caused from the surface tension between the two fluids that drives the instability (ref. [1] and [2]).

In order to find a solution without droplets formation we neglect the terms responsible of the instability, this will be discussed more in detail in the next section. In figure 1.1 we can see a base flow obtained numerically with the boundary elements method code developed in this project, from this is possible to perform a local stability analysis as it will be described in chapter 2.

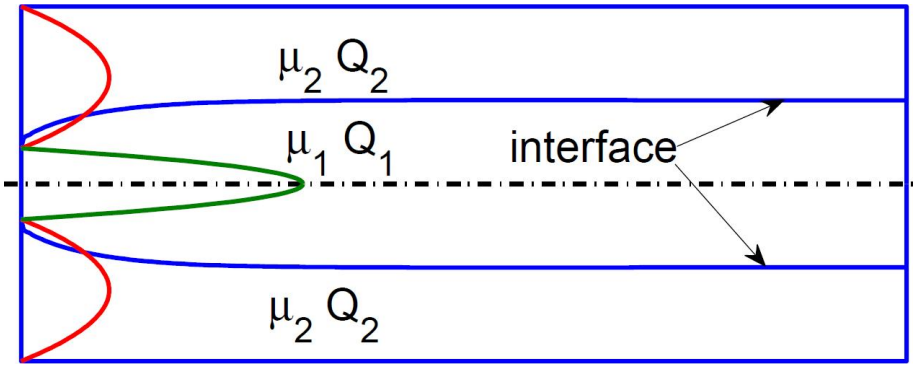

Figure 1.1: Base flow computed with boundary element method.

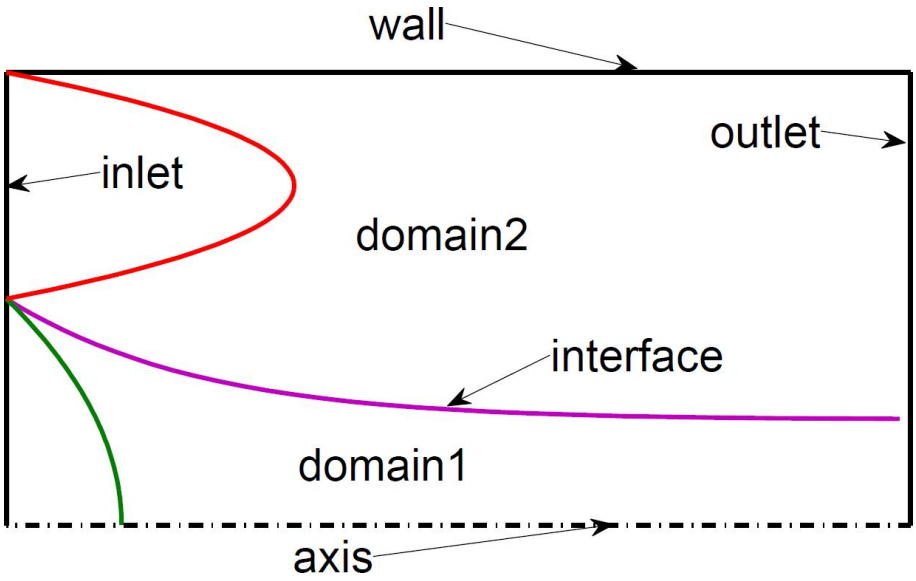

Figure 1.2: Observed domain.

1.2 Mathematical formulation of the problem

The phenomenon we want to observe allows us to do the following simplifying hypothesis

- Reynolds number tends to 0, this means that the inertial forces are negligible compared to the viscous forces
- Stationary flow
- Axisymmetric flow
- Gravity terms negligible

Considering the hypothesis, the governing equations of the problem are the stationary Stokes and continuity equations for incompressible flows for each fluid (domain 1 and 2, cf. figure 1.2), neglecting external forces:

$$\nabla P_i + \mu_i \nabla^2 \boldsymbol{U}_i = 0,$$

$$\nabla \cdot \boldsymbol{U}_i = 0, \qquad i = 1, 2$$

with the following boundary conditions: no slip at the wall and symmetry at the axis

$$U_z(R_2) = 0, \quad U_r(R_2) = 0, \quad \frac{\partial U_z}{\partial r} = 0, \quad U_r = 0, \quad \frac{\partial P}{\partial r} = 0.$$

The inner and outer domains are then coupled with the following interface conditions:
continuity of tangential stress

$$\boldsymbol{t}^T (\boldsymbol{\sigma}_2 - \boldsymbol{\sigma}_1)\, \boldsymbol{n} = 0,$$

where $\boldsymbol{t}$ and $\boldsymbol{n}$ are the tangential and normal unit vectors at the

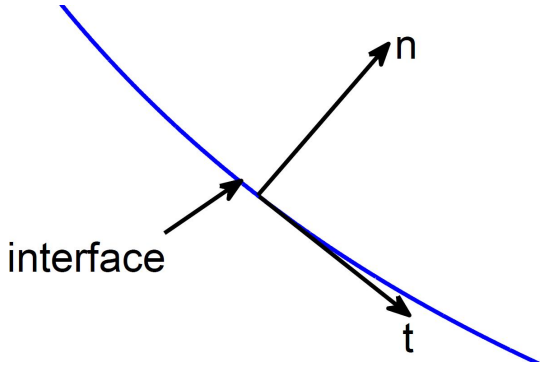

Figure 1.3: Normal and tangential unit vector to the interface.

interface (figure 1.3) and $\boldsymbol{\sigma}$ is the Newtonian stress tensor

$$\boldsymbol{\sigma} = \begin{pmatrix} -P_i + 2\mu_i \frac{\partial U_{z_i}}{\partial z} & \mu_i \left(\frac{\partial U_{z_i}}{\partial r} + \frac{\partial U_{r_i}}{\partial z} \right) \\ \mu_i \left(\frac{\partial U_{z_i}}{\partial r} + \frac{\partial U_{r_i}}{\partial z} \right) & -P_i + 2\mu_i \frac{\partial U_{r_i}}{\partial r} \end{pmatrix} \qquad i = 1, 2.$$

Discontinuity of normal stress due to surface tension

$$\boldsymbol{n}^T (\boldsymbol{\sigma}_2 - \boldsymbol{\sigma}_1) \boldsymbol{n} = \gamma \frac{1}{R_\parallel}.$$

Note that we use only the curvature given by the inflection of the interface in the meridional plane (the plane containing the axis), this is because we want to find a stable solution of the system (base flow) and the azimuthal component $1/R_\perp$ causes the instability of the flow.

What we are doing is to force the system to be stable, we will add $1/R_\perp$ later, together with the perturbations.
The continuity of the velocities across the interface reads:

$$U_{r1}(R_0) = U_{r2}(R_0), \quad U_{z1}(R_0) = U_{z2}(R_0),$$

and the impermeability of the interface is

$$U_r - U_z \frac{\partial R_0}{\partial z} = 0,$$

R_0 being the position of the interface.

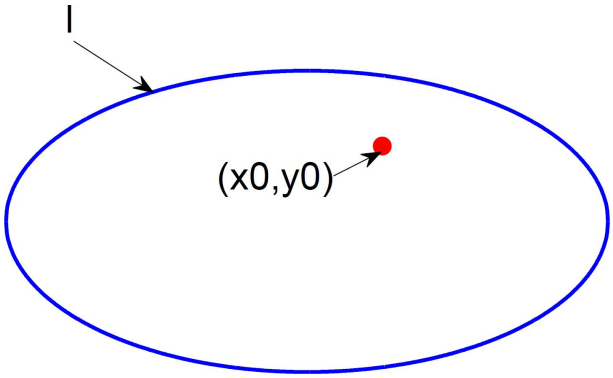

Figure 1.4: Example of the computation of the velocity in (x_0, y_0) with boundary integral equations.

1.3 Stokes as boundary integral equation

To treat interface problems like the one we want to analyze it is very convenient to reformulate the governing equations of the system as integral equations

$$\alpha \boldsymbol{u}(\boldsymbol{x}_0) = -\oint_l \boldsymbol{G}(\boldsymbol{x}, \boldsymbol{x}_0)\boldsymbol{f}(\boldsymbol{x})d\boldsymbol{l} + \mu \oint_l \boldsymbol{u}(\boldsymbol{x})\boldsymbol{T}(\boldsymbol{x}, \boldsymbol{x}_0)\boldsymbol{n}(\boldsymbol{x})d\boldsymbol{l}. \quad (1.1)$$

In equation 1.1 we have the boundary integral formulation of the Stokes equation given in [6] for a domain Ω closed from a boundary l.

$$\alpha = \begin{cases} 0 & \text{if } \boldsymbol{x}_0 \notin \Omega \\ 4\pi\mu & \text{if } \boldsymbol{x}_0 \in l \\ 8\pi\mu & \text{if } \boldsymbol{x}_0 \in \Omega - l \end{cases}$$

$\boldsymbol{G}$ and $\boldsymbol{T}$ are the Green's functions for an axisymmetic domain, from a physical point of view they propagate the information applied at the boundaries, in terms of stresses $\boldsymbol{f}$ and velocities $\boldsymbol{u}$, to the other parts of the domain ($\boldsymbol{n}$ is the unit vector normal to the boundary pointing inside the domain).

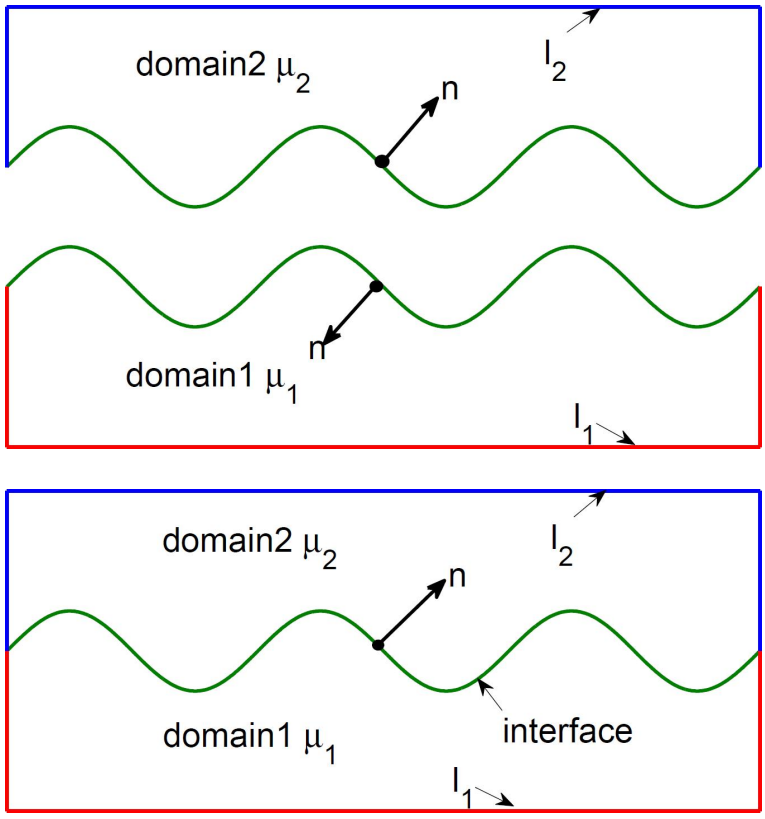

Figure 1.5: The two different domains coupled with the interface conditions.

For example to compute the velocity in (x_0, y_0) in figure 1.4 we just have to perform an integration along the boundary l using equation 1.1 with $\alpha = 8\pi\mu$. This has many advantages, for example there is no need to mesh the inner domain, on the other hand the numerical treatment of the integral equation can be problematic in some situations. As stated before, the implementation of this kind of equation for a problem with interface is quite straightforward, in fact we can imagine to have two separate domains in which we want to solve

Stokes equations (figure 1.5)

$$\begin{aligned}
\alpha \boldsymbol{u}(\boldsymbol{x}_0) = &- \int_{l_1} \boldsymbol{G}(\boldsymbol{x}, \boldsymbol{x}_0) \boldsymbol{f}(\boldsymbol{x}) d\boldsymbol{l} \\
&+ \mu_1 \int_{l_1} \boldsymbol{u}(\boldsymbol{x}) \boldsymbol{T}(\boldsymbol{x}, \boldsymbol{x}_0) \boldsymbol{n}(\boldsymbol{x}) d\boldsymbol{l} \\
&- \int_{int} \boldsymbol{G}(\boldsymbol{x}, \boldsymbol{x}_0) \boldsymbol{f}(\boldsymbol{x}) d\boldsymbol{l} \\
&+ \mu_1 \int_{int} \boldsymbol{u}(\boldsymbol{x}) \boldsymbol{T}(\boldsymbol{x}, \boldsymbol{x}_0) \boldsymbol{n}(\boldsymbol{x}) d\boldsymbol{l},
\end{aligned} \tag{1.2}$$

$$\begin{aligned}
\beta \boldsymbol{u}(\boldsymbol{x}_0) = &- \int_{l_2} \boldsymbol{G}(\boldsymbol{x}, \boldsymbol{x}_0) \boldsymbol{f}(\boldsymbol{x}) d\boldsymbol{l} \\
&+ \mu_2 \int_{l_2} \boldsymbol{u}(\boldsymbol{x}) \boldsymbol{T}(\boldsymbol{x}, \boldsymbol{x}_0) \boldsymbol{n}(\boldsymbol{x}) d\boldsymbol{l} \\
&- \int_{int} \boldsymbol{G}(\boldsymbol{x}, \boldsymbol{x}_0) \boldsymbol{f}(\boldsymbol{x}) d\boldsymbol{l} \\
&+ \mu_2 \int_{int} \boldsymbol{u}(\boldsymbol{x}) \boldsymbol{T}(\boldsymbol{x}, \boldsymbol{x}_0) \boldsymbol{n}(\boldsymbol{x}) d\boldsymbol{l}.
\end{aligned} \tag{1.3}$$

For these two domains we have the integral equations, 1.2 and 1.3, respectively. Summing 1.2 and 1.3 and taking into account the continuity of the velocities and the discontinuity of the normal stress at the interface $\Delta \boldsymbol{f} = \boldsymbol{f}_2 + \boldsymbol{f}_1 = \gamma(1/R_{\parallel})$, we obtain

$$\begin{aligned}
(\alpha + \beta) \boldsymbol{u}(\boldsymbol{x}_0) = &- \int_{l_1 + l_2} \boldsymbol{G}(\boldsymbol{x}, \boldsymbol{x}_0) \boldsymbol{f}(\boldsymbol{x}) d\boldsymbol{l} \\
&+ \mu_1 \int_{l_1} \boldsymbol{u}(\boldsymbol{x}) \boldsymbol{T}(\boldsymbol{x}, \boldsymbol{x}_0) \boldsymbol{n}(\boldsymbol{x}) d\boldsymbol{l} \\
&+ \mu_2 \int_{l_2} \boldsymbol{u}(\boldsymbol{x}) \boldsymbol{T}(\boldsymbol{x}, \boldsymbol{x}_0) \boldsymbol{n}(\boldsymbol{x}) d\boldsymbol{l} \\
&- \int_{int} \boldsymbol{G}(\boldsymbol{x}, \boldsymbol{x}_0) \Delta \boldsymbol{f}(\boldsymbol{x}) d\boldsymbol{l} \\
&+ (\mu_2 - \mu_1) \int_{int} \boldsymbol{u}(\boldsymbol{x}) \boldsymbol{T}(\boldsymbol{x}, \boldsymbol{x}_0) \boldsymbol{n}(\boldsymbol{x}) d\boldsymbol{l},
\end{aligned} \tag{1.4}$$

where

$$\alpha+\beta=\begin{cases}0 & \text{if } \boldsymbol{x}_0 \notin \Omega_1+\Omega_2\\ 4\pi\mu_1 & \text{if } \boldsymbol{x}_0 \in l_1\\ 4\pi\mu_2 & \text{if } \boldsymbol{x}_0 \in l_2\\ 8\pi\mu_1 & \text{if } \boldsymbol{x}_0 \in \Omega_1 - l_1\\ 8\pi\mu_2 & \text{if } \boldsymbol{x}_0 \in \Omega_2 - l_2\\ 4\pi(\mu_1+\mu_2) & \text{if } \boldsymbol{x}_0 \in \text{interface.}\end{cases}$$

The signs in equation 1.4, in the part regarding the interface, come from having considered positive the normal to the interface pointing inside the domain 2 (figure 1.5). Once the governing equation is determined, we impose the boundary conditions in order to close the problem. In every point of the domain we have four variables, stresses and velocities in the axial and radial direction, in every point of the boundary we impose two of them. Looking at figure 1.2 we impose

- no slip condition at wall
- uniform normal stress and zero radial velocity at the outlet
- bi-Poiseuille axial velocity and zero radial velocity at the inlet

there is no need to impose anything on the axis because the Green's functions already take in account the axisymmetric character of the problem.

1.4 Numerical method

In this section it is explained how the integral equation 1.4 is solved numerically. In figure 1.6 we can see how we discretize the boundaries. The position of the interface in the figure 1.6 is a guess position from which we start the calculation, what we do is to find the velocities in the interface nodes and move them with these velocities after having fixed a Δt.

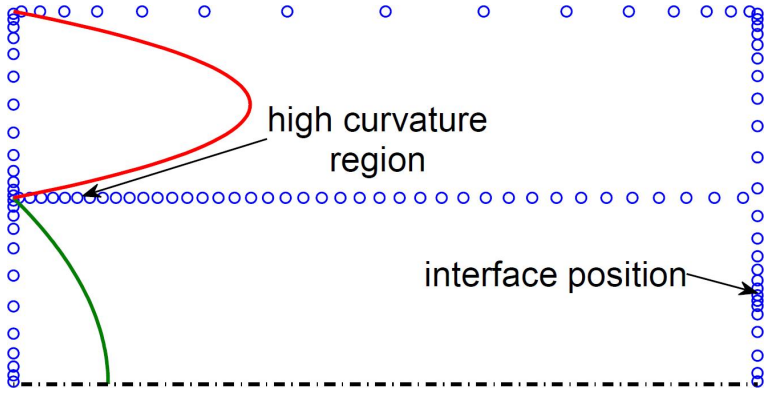

Figure 1.6: Discretization of the problem.

This process is carried out until the velocities in these nodes satisfy the interface condition of impermeability, velocity normal to the interface equal to zero (very small in our discretized case). In figure 1.7 we see an example of evolution of the interface after a few iterations. This approach is very good from a physical point of view, because it uses a physical criterion to move the interface, on the other hand we must be very careful because of its explicit nature.

In fact, if we take too high Δt the information given from one node is moved too far (moving the node itself with its velocity) and this gives rise to numerical oscillations. The nodes distribution is done with the aim to have a finer mesh where we have discontinuous changes in viscosity (where the interface touches inlet and outlet) and where we have a change in the boundary condition imposed (corner points). We also have a higher density of nodes at the interface close to the inlet, where the interface will bend more and the computation of the curvature will need to be more accurate. In every node in figure 1.6 a six points Gauss integration of the Green's functions is performed, assuming stresses and velocities constants (cf. figure 1.8).

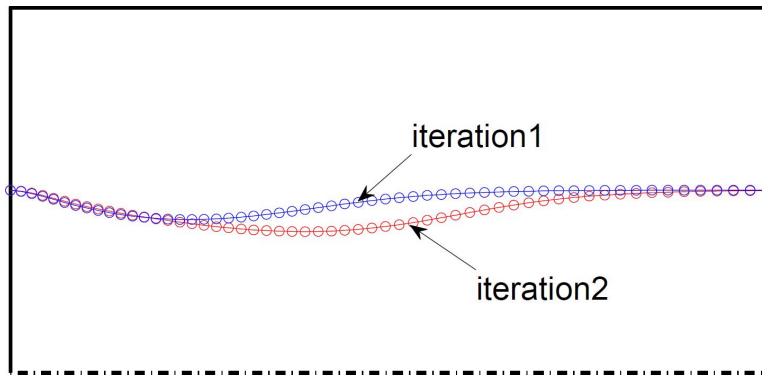

Figure 1.7: Iterative process to find the interface position.

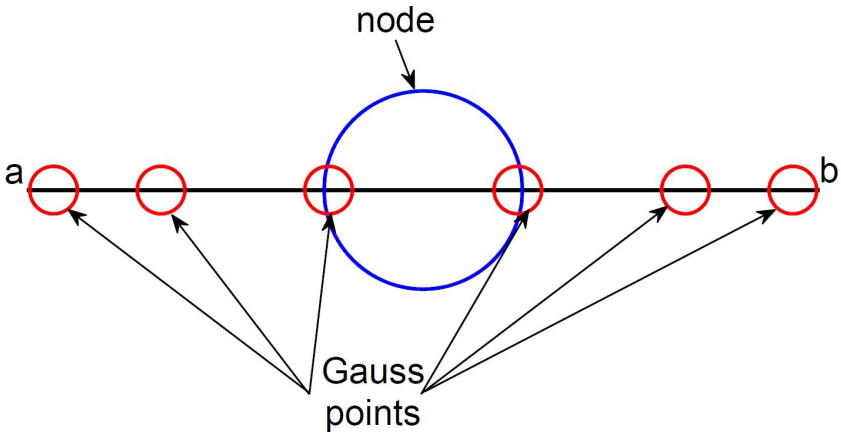

Figure 1.8: Six points Gauss integration for every node.

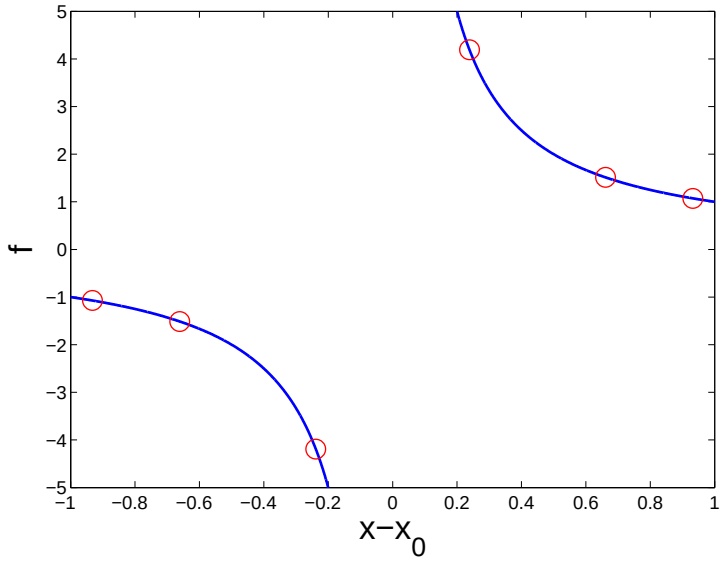

Figure 1.9: Green's function behavior around the singularity.

Hence on the single node we have

$$\int_a^b \boldsymbol{G}(\boldsymbol{x},\boldsymbol{x}_0)\boldsymbol{f}(\boldsymbol{x})d\boldsymbol{l} \approx \boldsymbol{f}_{ab}\int_a^b \boldsymbol{G}(\boldsymbol{x},\boldsymbol{x}_0)d\boldsymbol{l} \approx \boldsymbol{f}_{ab}\sum_{i=1}^{6}\boldsymbol{G}(\boldsymbol{x}_i,\boldsymbol{x}_0)w_i,$$

where w_i are the Gauss weights associated to the different Gauss points. What we just described is the standard treatment of the integration around a node but when $\boldsymbol{x} \to \boldsymbol{x}_0$ we have to do something different. In that case in fact the Green's functions exhibit a singular behavior. Let's take a look at the Green's functions more in detail:

$$\boldsymbol{G} = \begin{pmatrix} G_{xx} & G_{xy} \\ G_{yx} & G_{yy} \end{pmatrix}, \boldsymbol{T}_x = \begin{pmatrix} T_{xxx} & T_{xxy} \\ T_{xyx} & T_{xyy} \end{pmatrix}, \boldsymbol{T}_y = \begin{pmatrix} T_{yxx} & T_{yxy} \\ T_{yyx} & T_{yyy} \end{pmatrix}.$$

Except for G_{xx} and G_{yy}, all the other components have a qualitative behavior like the function in figure 1.9 around the singularity in $\boldsymbol{x} = \boldsymbol{x}_0$. In these cases the error we introduce integrating on the Gauss

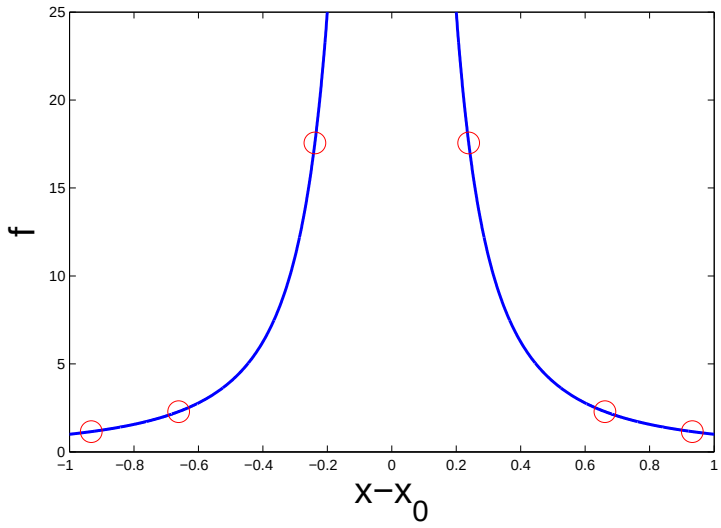

Figure 1.10: Green's function behavior around the singularity.

point is zero because the values of the integrals on the right and on the left of the singularity are equals with opposite signs. For G_{xx} and G_{yy} the approach is different, in fact they have a behavior like that illustrated in figure 1.10, and this creates an important problem in term of accuracy of the numerical integral, because the contribution to the integral of the interval between the closer Gauss point to the singularity and the singularity itself is not taken in account. Let's look at the analytical expression of G_{xx} where $\boldsymbol{x} = (x, r)$ and $\boldsymbol{x}_0 = (x_0, r_0)$

$$G_{xx}(\boldsymbol{x}, \boldsymbol{x}_0) = \frac{4r}{\sqrt{(x - x_0)^2 + (r + r_0)^2}} \left(F + \frac{(x - x_0)^2}{(r - r_0)^2} E \right),$$

The term that goes to infinity is F, what we do is to use a local analytical expression for it, in [6] is proposes

$$F \approx \ln |\boldsymbol{x} - \boldsymbol{x}_0| + ... \qquad E \approx 1 + ...$$

Taking the first order expansion we obtain the local approximation

$$G_{xx}(\boldsymbol{x}, \boldsymbol{x}_0) \approx -2 \ln |\boldsymbol{x} - \boldsymbol{x}_0| + 1, \tag{1.5}$$

since 1.5 is analytically integrable, we can write

$$\begin{aligned}\int_a^b G_{xx}(\boldsymbol{x}, \boldsymbol{x}_0) d\boldsymbol{l} = &\int_a^b (G_{xx}(\boldsymbol{x}, \boldsymbol{x}_0) + 2 \ln |\boldsymbol{x} - \boldsymbol{x}_0| + 1) d\boldsymbol{l} + \\ &\int_a^b (-2 \ln |\boldsymbol{x} - \boldsymbol{x}_0| + 1) d\boldsymbol{l} = \\ &\int_a^b (G_{xx}(\boldsymbol{x}, \boldsymbol{x}_0) + 2 \ln |\boldsymbol{x} - \boldsymbol{x}_0| + 1) d\boldsymbol{l} \\ &+ \big[-2|\boldsymbol{x} - \boldsymbol{x}_0| \ln |\boldsymbol{x} - \boldsymbol{x}_0| + 3|\boldsymbol{x} - \boldsymbol{x}_0| \big]_a^b.\end{aligned}$$

In this way we subtract the diverging part from the numerical integral and add it in an analytical form, keeping a good accuracy. Now that we have the integrals of the Green's functions for every nodes, we perform a numerical integral of the entire boundary l using the rectangle method. If we have N nodes we obtain

$$\oint_l \boldsymbol{G}(\boldsymbol{x}, \boldsymbol{x}_0) \boldsymbol{f}(\boldsymbol{x}) d\boldsymbol{l} \approx \sum_{n=1}^{N} \boldsymbol{f}_n \left(\sum_{i=1}^{6} \boldsymbol{G}(\boldsymbol{x}_i, \boldsymbol{x}_0) w_i \right)_n .$$

This leads to a linear problem ($2N$ unknowns in $2N$ equations) that once solved provides the velocities and the stresses on the boundaries and on the interface. These results are used as boundary conditions to run a FreeFem [7] simulation using the finite elements method. We have chosen this approach because it would have taken too long (in the frame of this project) to have access to all the quantities we need to perform local stability analysis (stress tensor gradient) with the boundary elements method. On the other hand with the boundary elements method it is much easier to find the interface position, in figure 1.11 we can see a convergence study on the error on the interface position in the fully developed region computed with

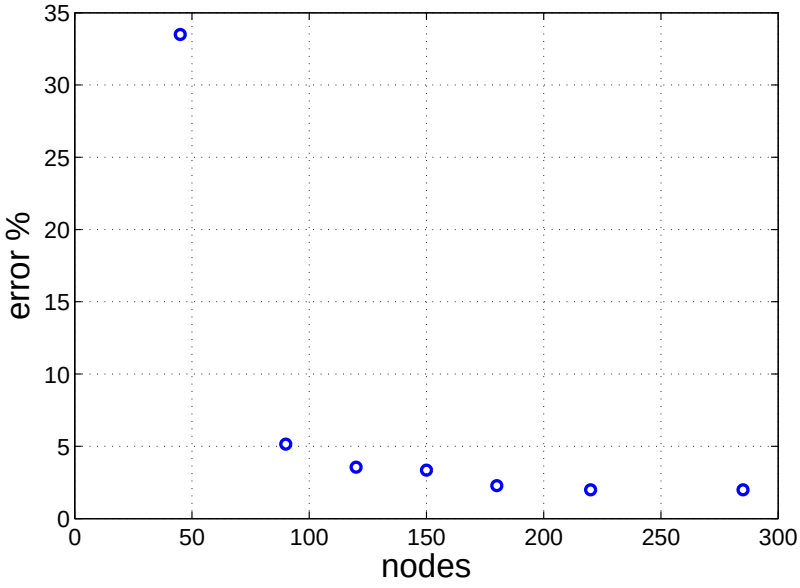

Figure 1.11: Convergence study.

Figure 1.12: FreeFem mesh for domain 1 and 2.

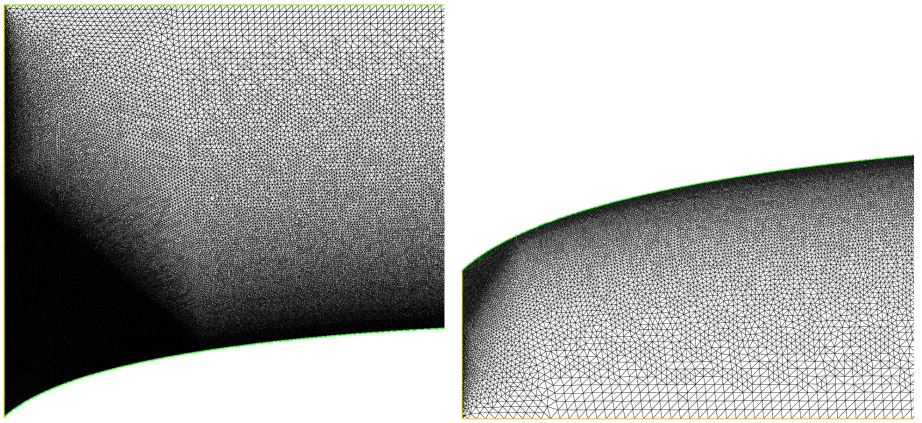

Figure 1.13: Zoom of FreeFem mesh close to the inlet for domain 1 and 2.

the boundary elements method, compared to the analytical solution.

FreeFem computations have been carried on by Edouard Boujo a former Phd student at LFMI-EPFL; in these computations domain 1 and 2 are computed separately like two different flows, in figure 1.12 we can see the mesh in FreeFem based on the domain configuration found with the boundary elements method, imposing the velocities as boundaries conditions, in figure 1.13 we may notice how the mesh is finer close to inlet where our study is focused. In this way we find the pressure field (figure 1.14), axial and radial velocities fields (figure 1.15 and 1.16) in all the domain and we obtain all the quantities we need to perform local stability analysis.

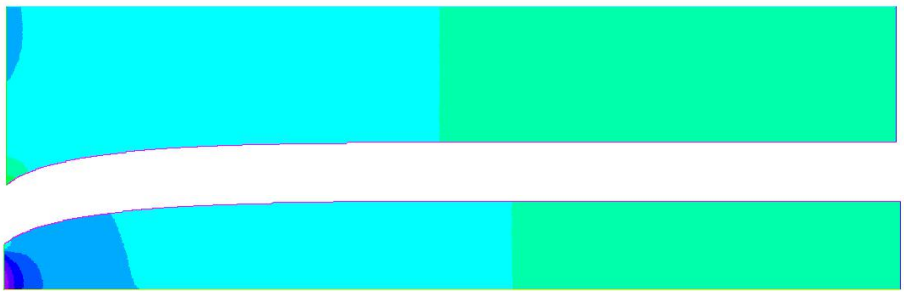

Figure 1.14: Pressure field for domain 1 and 2.

Figure 1.15: Axial velocity field for domain 1 and 2.

Figure 1.16: Radial velocity field for domain 1 and 2.

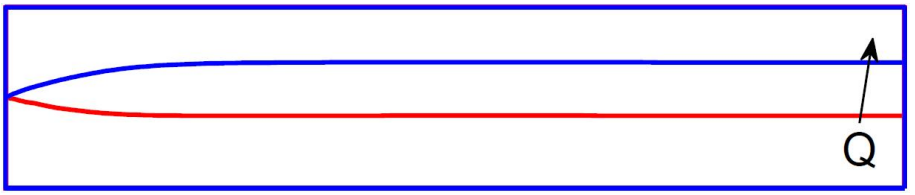

Figure 1.17: Interface position for different flow rate ratio, $\lambda = 0.6$, $Ka = 10$.

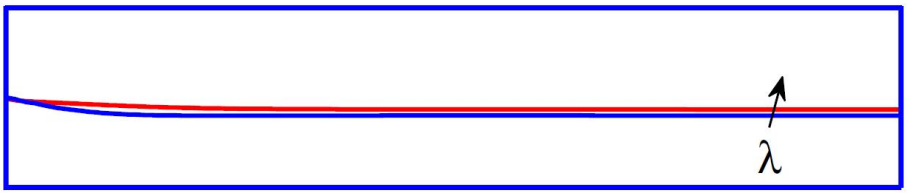

Figure 1.18: Interface position for different viscosity ratio, $Q = 0.5$, $Ka = 10$.

1.5 Results from the base flow calculations

The problem is treated in function of three dimensionless numbers: the flow rate ratio, the viscosity ratio and the capillary number

$$Q = \frac{Q_1}{Q_2}, \quad \lambda = \frac{\mu_1}{\mu_2}, \quad Ka = \frac{\partial_z p R_2^2}{\gamma}.$$

Here are reported some flow configuration obtained with the boundary elements method code previously mentioned. As for the analytical description we can notice how the interface position at the outlet varies when we change flow rate and viscosity ratios. Increasing the flow rate and the viscosity ratio will move the interface toward the wall and vice versa, we can observe this behavior in figure 1.17 and 1.18. The duration of the calculations is very dependent on the value of the surface tension and on the velocity of the flow; these parameters are taken into account with the capillary number. The larger the pressure gradient is the more the velocity is high and the movement

of the interface is fast; then the calculation is fast. Opposite behavior is found when the surface tension is large, because this tends to make the computation numerically unstable.

Chapter 2

Local linear stability analysis

2.1 How does it work

The aim of the stability analysis is to understand if a certain physical configuration is stable when we apply small perturbations on it. The configurations to which we are going to add perturbations are called fixed points, this means that they wouldn't change their state if not perturbed. One common example of stable and unstable configuration is the ball at the bottom of the valley or on the top of a mountain (figure 2.1). In the first case if we move the ball of an infinitesimal space (small perturbation), the ball will return in the initial position after an oscillation around the fixed point. In the second case the

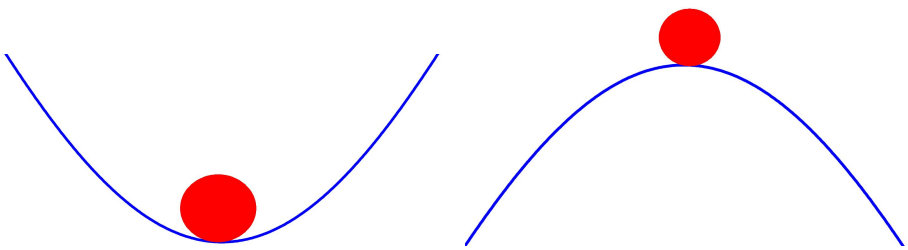

Figure 2.1: Stable and unstable configurations.

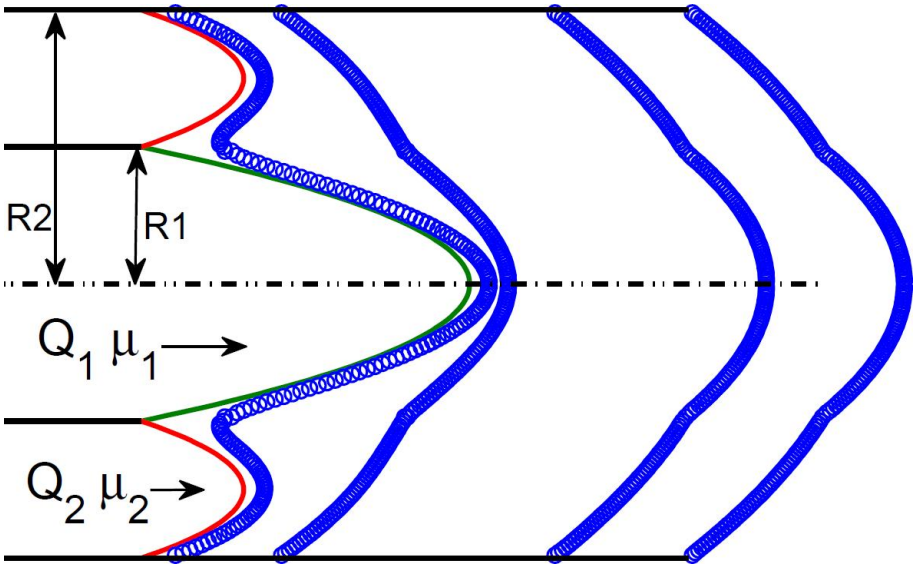

Figure 2.2: Physical configuration, in blue velocities profile computed with the MATLAB code developed in the project.

ball will start to fall down until it reaches a valley (another stable solution).

In our case the fixed point is a stationary and stable solution (base flow) of the flow we are considering. What we want to understand is if this flow maintains its configuration once it has been perturbed. Taking small perturbations of pressure, velocities and interface position compared with the order of magnitude of the quantities of the base flow, it is possible to linearize the governing equations for the perturbations around the fixed point (base flow) and look for their behavior around it.

When the stability analysis is performed on a flow which is considered completely developed, a local stability analysis is being performed. In our case we will consider a coaxial jet, we will perform this kind of analysis in different sections of the developing region, taking each time the velocity profile of the section we are studying (figure

2.2). We are thus doing a "local" analysis of a (mildly) non-parallel flow.

2.2 Mathematical formulation of the problem

The assumptions of the local analysis lead to some important simplifications such as

$$U_r = 0, \qquad \frac{\partial}{\partial z} = 0,$$

from a physical point of view this means that the radial velocity is very small everywhere and the evolution of the flow in the axial direction is slow compared to the wavelength of the perturbation. As it was stated in the previous section, small perturbations will be summed to the quantities of the unperturbed flow, the base flow (capitol letters for the base flow quantities). That is

$$\begin{pmatrix} \bar{U}_z \\ \bar{U}_r \\ \bar{P} \\ \bar{R} \end{pmatrix} = \begin{pmatrix} U_z + \varepsilon u_z \\ 0 + \varepsilon u_r \\ P + \varepsilon p \\ R_0 + \varepsilon \eta \end{pmatrix} \qquad \text{with} \qquad \varepsilon \ll 1.$$

Replacing the unperturbed quantities with the perturbed ones in the governing equations it is found

$$r : -\frac{\partial P}{\partial r} - \varepsilon\frac{\partial p}{\partial r} + \mu\left[\frac{1}{r}\frac{\partial}{\partial r}\left(r\varepsilon\frac{\partial u_r}{\partial r}\right) + \varepsilon\frac{\partial^2 u_r}{\partial z^2} - \varepsilon\frac{u_r}{r^2}\right] = 0,$$

$$z : -\frac{\partial P}{\partial z} - \varepsilon\frac{\partial p}{\partial z} + \mu\left[\frac{1}{r}\frac{\partial}{\partial r}\left(r\frac{\partial U_z}{\partial r} + r\varepsilon\frac{\partial u_z}{\partial r}\right) + \frac{\partial^2 U_z}{\partial z^2} + \varepsilon\frac{\partial^2 u_z}{\partial z^2}\right] = 0,$$

$$\varepsilon\frac{\partial u_r}{\partial r} + \varepsilon\frac{u_r}{r} + \frac{\partial U_z}{\partial z} + \varepsilon\frac{\partial u_z}{\partial z} = 0.$$

Canceling the part verifying the governing equations for the base flow and taking only the terms of order ε, we reach the linearized equation

for the perturbations

$$r : -\frac{\partial p}{\partial r} + \mu\left[\frac{1}{r}\frac{\partial}{\partial r}\left(r\frac{\partial u_r}{\partial r}\right) + \frac{\partial^2 u_r}{\partial z^2} - \frac{u_r}{r^2}\right] = 0,$$

$$z : -\frac{\partial p}{\partial z} + \mu\left[\frac{1}{r}\frac{\partial}{\partial r}\left(r\frac{\partial u_z}{\partial r}\right) + \frac{\partial^2 u_z}{\partial z^2}\right] = 0,$$

$$\frac{\partial u_r}{\partial r} + \frac{u_r}{r} + \frac{\partial u_z}{\partial z} = 0.$$

In the same way we obtain the linearized boundary conditions

$$\text{no slip at the wall:} \qquad u_z(R_2) = 0, \quad u_r(R_2) = 0,$$

$$\text{symmetry on the axis:} \qquad u_r(0) = 0, \quad \left.\frac{\partial u_z}{\partial r}\right|_0 = 0, \quad \left.\frac{\partial p}{\partial r}\right|_0 = 0.$$

For the linearized interface conditions we have to consider the perturbation of the interface itself, than the conditions should be imposed at $R_0 + \varepsilon\eta$.

Let's see how these conditions should be applied, for example for the continuity of axial velocity

$$U_{z_1}(R_0 + \varepsilon\eta) + \varepsilon u_{z_1}(R_0 + \varepsilon\eta) = U_{z_2}(R_0 + \varepsilon\eta) + \varepsilon u_{z_2}(R_0 + \varepsilon\eta). \quad (2.1)$$

The problem is that from the computation of the base flow we don't know the position of the perturbed interface. We can however carry out a Taylor expansion around R_0, the unperturbed interface point, to extract the quantities in the perturbed location (figure 2.3). Let's see an example for a generic function f

$$f(R_0 + \varepsilon\eta) = f(R_0) + \left.\frac{\partial f}{\partial r}\right|_{R_0} \varepsilon\eta.$$

In our case we obtain, for the continuity of the axial velocity

$$\begin{aligned} U_{z_1}(R_0 + \varepsilon\eta) + \varepsilon u_{z_1}(R_0 + \varepsilon\eta) =& U_{z_1}(R_0) + \left.\frac{\partial U_{z_1}}{\partial r}\right|_{R_0} \varepsilon\eta \\ &+ \varepsilon u_{z_1}(R_0) + \left.\frac{\partial u_{z_1}}{\partial r}\right|_{R_0} \varepsilon^2\eta, \end{aligned}$$

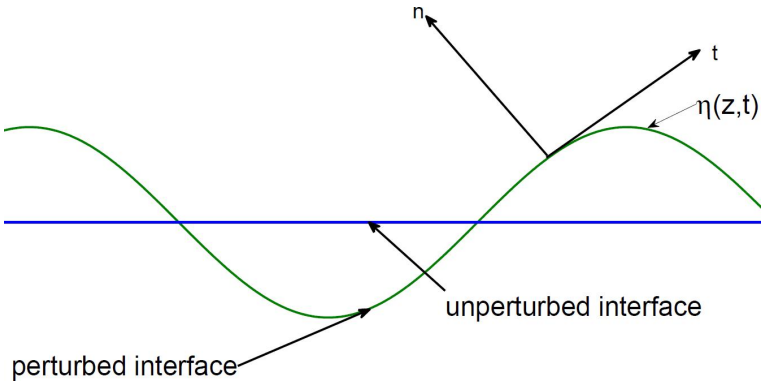

Figure 2.3: "Flattening" hypothesis.

and similarly for the outer domain. Replacing in 2.1 and neglecting the terms which satisfy the base flow interface conditions and the terms of order ε^2 and smaller, we have:

$$u_{z_1}(R_0) + \frac{\partial U_{z_1}}{\partial r}\Big|_{R_0} \eta = u_{z_2}(R_0) + \frac{\partial U_{z_2}}{\partial r}\Big|_{R_0} \eta.$$

Following the same process we come to the other linearized interface conditions,
the continuity of radial velocities

$$u_{r_1}(R_0) + \frac{\partial U_{r_1}}{\partial r}\Big|_{R_0} \eta = u_{r_2}(R_0) + \frac{\partial U_{r_2}}{\partial r}\Big|_{R_0} \eta,$$

that becomes $u_{r_1}(R_0) = u_{r_2}(R_0)$ because $U_r = 0$ everywhere.
The continuity of the tangential stress reads:

$$\boldsymbol{t}^T[(\boldsymbol{\sigma}_2 + \varepsilon \boldsymbol{e}_2) - (\boldsymbol{\sigma}_1 + \varepsilon \boldsymbol{e}_1)]\boldsymbol{n} = 0,$$

where $\boldsymbol{e}$ is the Newtonian stress tensor for the perturbation and $\boldsymbol{n}$ and $\boldsymbol{t}$ are the perturbed normal and tangential unit vectors to the interface (figure 2.3)

$$n = \left(-\frac{\partial \eta}{\partial z} \quad , \quad 1 \right)^T, \qquad t = \left(1 \quad , \quad \frac{\partial \eta}{\partial z} \right)^T,$$

we then come to write:

$$\left(\mu_2\frac{\partial^2 U_{z_2}}{\partial r^2}-\mu_1\frac{\partial^2 U_{z_1}}{\partial r^2}\right)\eta+\mu_2\left(\frac{\partial u_{z_2}}{\partial r}+\frac{\partial u_{r_2}}{\partial z}\right)-\mu_1\left(\frac{\partial u_{z_1}}{\partial r}+\frac{\partial u_{r_1}}{\partial z}\right)=0,$$

The balance of normal stress reads:

$$\boldsymbol{n}^T[(\boldsymbol{\sigma}_2+\varepsilon\boldsymbol{e}_2)-(\boldsymbol{\sigma}_1+\varepsilon\boldsymbol{e}_1)]\boldsymbol{n}=\gamma\left(\frac{1}{\bar{R}_\parallel}+\frac{1}{\bar{R}_\perp}\right),$$

that finally leads to

$$\left(\frac{\partial P_1}{\partial r}-\frac{\partial P_2}{\partial r}\right)\eta+2\left(\mu_1\frac{\partial U_{z_1}}{\partial r}-\mu_2\frac{\partial U_{z_2}}{\partial r}\right)\frac{\partial\eta}{\partial z}+p_1-p_2$$
$$-2\mu_1\frac{\partial u_{z_1}}{\partial r}+2\mu_2\frac{\partial u_{z_2}}{\partial r}=-\gamma\left(\frac{\eta}{R_0^2}+\frac{\partial^2\eta}{\partial z^2}\right).$$

Finally, the kinematic interface condition is:

$$\left.\frac{\partial\eta}{\partial t}\right|_{R_0}=u_{r_1}(R_0)-U_z^{int}\left.\frac{\partial\eta}{\partial z}\right|_{R_0}.$$

The unknowns of the problem are than substituted with the modal expansion

$$u_r=\hat{u}_r(r)e^{i(kz-\omega t)},\qquad u_z=\hat{u}_z(r)e^{i(kz-\omega t)},$$
$$p=\hat{p}(r)e^{i(kz-\omega t)},\qquad \eta=\hat{\eta}e^{i(kz-\omega t)}.$$

Writing the unknowns in this way we split the radial evolution of the perturbations and the axial and temporal evolutions of the perturbations, the latter are included in the exponential term.

What we will do is to perturb the system in the space along the axial direction, choosing a certain wavelength, trough k and see how it will react in time, looking at the ω we will find. More in detail we set a linear system containing the discretized Stokes equations for domain 1 and 2 coupled with the interface condition equations. The system has the following form:

$$A\varphi=0,$$

where φ is the unknowns vector

$$\varphi = \begin{pmatrix} \hat{u}_{r_1} & \hat{u}_{z_1} & \hat{p}_1 & \hat{u}_{r_2} & \hat{u}_{z_2} & \hat{p}_2 & \hat{\eta} \end{pmatrix}^T,$$

and A is the matrix of the coefficients of the linear system, which we can write schematically as:

$$A = \begin{pmatrix} [Domain \quad 1] & [0] \\ [0] & [Domain \quad 2] \\ [interface & conditions] \end{pmatrix}$$

This system has non trivial solution if and only if $det(A) = 0$; once k is fixed, the previous condition leads to an eigenvalue problem for ω. We can then find the complex parameter that determines the temporal evolution of the perturbations

$$\omega = \omega_r + i\omega_i.$$

From the way in which the modal expansion is formulated, the complex part of ω will give the temporal evolution of the perturbation, i.e. its growth rate, the real part will give the temporal frequency of the perturbation.

2.3 Numerical method

In this project, the system shown in the previous section is solved numerically with a in-house MATLAB code using a spectral method. The code, first developed by Francesco Viola (former Phd student at the LFMI-EPFL) to perform stability analysis on flows at high Reynolds number, has been adapted for problems with interfaces at low Reynolds numbers. Replacing the unknowns of the problem with their modal expansion we obtain, for a function $f(r, z, t) = \hat{f}(r)e^{i(kz-\omega t)}$

$$\frac{\partial f}{\partial z} = \hat{f}(r)ike^{i(kz-\omega t)}, \qquad \frac{\partial f}{\partial t} = -\hat{f}(r)i\omega e^{i(kz-\omega t)}, \qquad \frac{\partial f}{\partial r} = \frac{\partial \hat{f}}{\partial r}e^{i(kz-\omega t)},$$

this leads to a system of ODEs in r. The governing equation are modified as follow:
Stokes equation

$$r: \quad \mu_i\left(\frac{1}{r}\frac{d\hat{u}_{r_j}}{dr}+\frac{d^2\hat{u}_{r_j}}{dr^2}-\hat{u}_{r_i}k^2-\frac{\hat{u}_{r_j}}{r^2}\right)-\frac{dp_j}{dr}=0,$$

$$z: \quad \mu_i\left(\frac{1}{r}\frac{d\hat{u}_{z_j}}{dr}+\frac{d^2\hat{u}_{z_j}}{dr^2}-\hat{u}_{z_j}k^2\right)-ikp_j=0,$$

mass continuity

$$\frac{\hat{u}_{r_j}}{r}+\frac{d\hat{u}_{r_j}}{dr}+ik\hat{u}_{z_j}=0, \qquad j=1,2$$

impermeability of the interface

$$-i\omega\hat{\eta}=\hat{u}_{r_1}-U_z^{int}kz\hat{\eta},$$

no slip condition at the wall

$$\hat{u}_{r_2}(R_2)=0, \qquad \hat{u}_{z_2}(R_2)=0,$$

symmetry condition at the axis:

$$\hat{u}_{r_1}(0)=0, \quad \left.\frac{\partial\hat{u}_{z_1}}{\partial r}\right|_0=0, \quad \left.\frac{\partial\hat{p}_1}{\partial r}\right|_0=0,$$

continuity of the velocity at the interface

$$\hat{u}_{r_1}(R_0)=\hat{u}_{r_2}(R_0),$$

$$\hat{u}_{z1}(R_0)+\left.\frac{\partial U_{z_1}}{\partial r}\right|_{R_0}\hat{\eta}=\hat{u}_{z2}(R_0)+\left.\frac{\partial U_{z_2}}{\partial r}\right|_{R_0}\hat{\eta},$$

continuity of tangential stress

$$\left(\mu_2\frac{\partial^2U_{z_2}}{\partial r^2}-\mu_1\frac{\partial^2U_{z_1}}{\partial r^2}\right)\hat{\eta}+\mu_2\left(\frac{\partial\hat{u}_{z_2}}{\partial r}+ik\hat{u}_{r_2}\right)-\mu_1\left(\frac{\partial\hat{u}_{z_1}}{\partial r}+ik\hat{u}_{r_1}\right)=0,$$

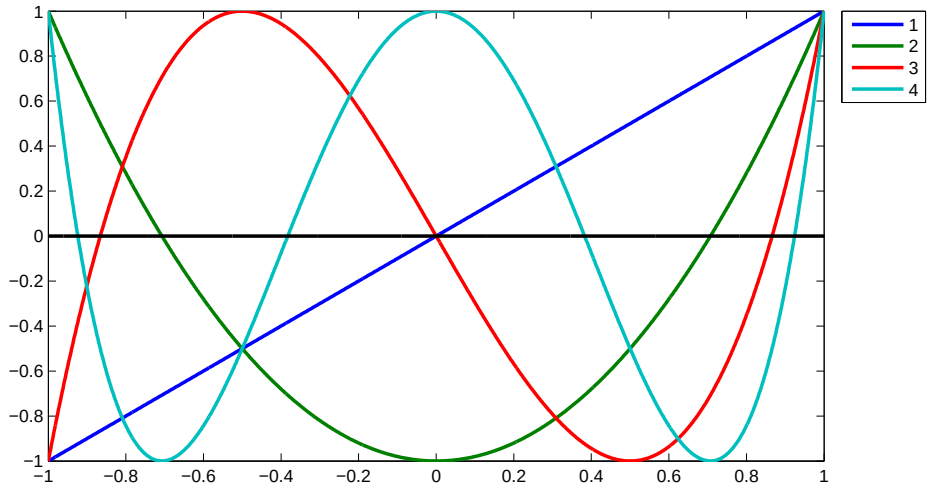

Figure 2.4: Chebyshev polynomials of different degree.

balance of normal stress

$$\left(\frac{\partial P_1}{\partial r} - \frac{\partial P_2}{\partial r}\right)\hat{\eta} + 2\left(\mu_1 \frac{\partial U_{z_1}}{\partial r} - \mu_2 \frac{\partial U_{z_2}}{\partial r}\right) ik\hat{\eta} + \hat{p}_1 - \hat{p}_2$$
$$-2\mu_1 \frac{\partial \hat{u}_{z_1}}{\partial r} + 2\mu_2 \frac{\partial \hat{u}_{z_2}}{\partial r} = -\gamma\left(\frac{1}{R_0^2} - k^2\right)\hat{\eta}.$$

To perform the derivatives the domain is discretized in the radial direction, thus every ODE become a system of linear equation. To ensure a good accuracy without high computational cost the code employs Chebyshev polynomials.

The nodes are determined from the roots of the Chebyshev polynomial, they are as much as the degree of the polynomial. In figure 2.4 we can see Chebyshev polynomial of different degrees. Using this kind of discretization, every node gives information to all the others. The computation of the derivate of a generic function f will be given by the product between a full matrix times the vector containing the

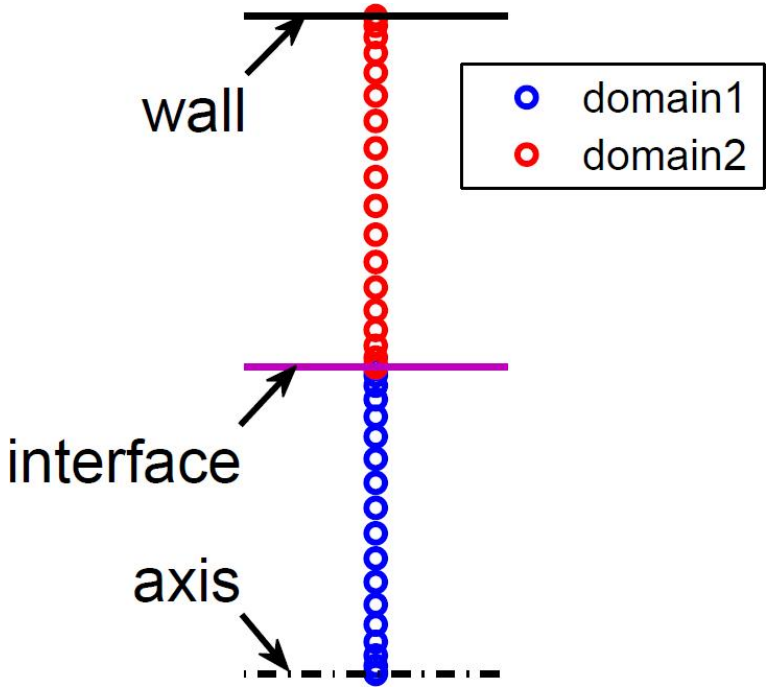

Figure 2.5: Fitting the nodes in the physical domain.

values of f in the nodes.

$$\begin{pmatrix} f_1' \\ f_2' \\ \vdots \\ f_n' \end{pmatrix} = \begin{pmatrix} a_{11} & a_{12} & \dots & a_{1n} \\ a_{21} & a_{22} & \dots & a_{2n} \\ \vdots & \vdots & \ddots & \vdots \\ a_{n1} & a_{n2} & \dots & a_{nn} \end{pmatrix} \begin{pmatrix} f_1 \\ f_2 \\ \vdots \\ f_n \end{pmatrix}$$

The main advantage of this method is a really fast convergence (exponential if the function is smooth), this makes the method convenient even if we have fully populated matrices. A drawback of the spectral collocation method is the fact that the distribution of the nodes is determined from the polynomials and it is not straightforward to modify it.

In our code we have just changed the starting and ending point

of the polynomial (previously defined between -1 and 1) performing a linear mapping (figure 2.5) to fit the physical domain we had to analyze. Calling s the original independent variable of the Chebyshev polynomial and R_0 the position of the interface, the physical coordinate is for the domain 1 and 2 respectively

$$r_1 = \frac{s+1}{2} R_0, \qquad r_2 = R_0 + (R_2 - R_0)\frac{s+1}{2}.$$

From this change of coordinate also the derivatives vary:
first derivatives

$$\frac{\partial f}{\partial r_1} = \frac{\partial f}{\partial s}\frac{\partial s}{\partial r_1} = \frac{\partial f}{\partial s}\frac{2}{R_0},$$
$$\frac{\partial f}{\partial r_2} = \frac{\partial f}{\partial s}\frac{\partial s}{\partial r_2} = \frac{\partial f}{\partial s}\frac{2}{R_2 - R_0},$$

second derivatives, taking in account that s is a linear function of r

$$\frac{\partial^2 f}{\partial r_1^2} = \frac{\partial f}{\partial s \partial r_1}\frac{\partial s}{\partial r_1} + \frac{\partial f}{\partial s}\frac{\partial^2 s}{\partial r_1^2} = \frac{\partial^2 f}{\partial s^2}\left(\frac{\partial s}{\partial r_1}\right)^2 = \frac{\partial^2 f}{\partial s^2}\frac{4}{R_0^2},$$
$$\frac{\partial^2 f}{\partial r_2^2} = \frac{\partial^2 f}{\partial s^2}\frac{4}{(R_2 - R_0)^2}.$$

In figure 2.6 we can see a study on the convergence of the method that considers the error on the maximum value of ω_i compared with the analytical solution in the completely developed region. This demonstrates that a resolution with 20 Chebyshev points (for each domain) is perfectly adequate for our purpose. The linear system is finally structured in the following way

$$\begin{pmatrix} [Stokes\ \ r\ direction]_1 & 0 & 0 \\ [Stokes\ \ z\ direction]_1 & 0 & 0 \\ [Continuity]_1 & 0 & 0 \\ 0 & [Stokes\ \ r\ direction]_2 & 0 \\ 0 & [Stokes\ \ z\ direction]_2 & 0 \\ 0 & [Continuity]_2 & 0 \\ impermeability & of\ \ the\ \ interface & \end{pmatrix} \begin{pmatrix} [\hat{u}_{r_1}] \\ [\hat{u}_{z_1}] \\ [\hat{p}_1] \\ [\hat{u}_{r_2}] \\ [\hat{u}_{z_2}] \\ [\hat{p}_2] \\ \hat{\eta} \end{pmatrix} = 0.$$

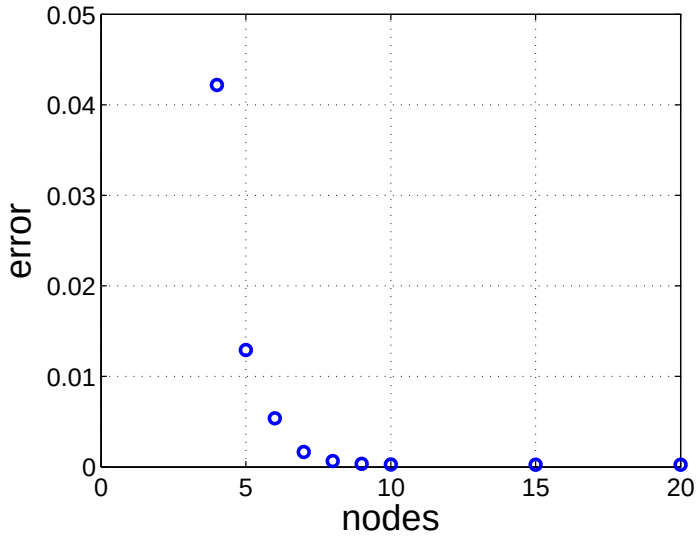

Figure 2.6: Convergence study.

The rows in squared bracket are the ones that contain derivatives in the radial direction, each of those is actually formed from as many lines as the number of nodes. The first and last lines of these sections contain the boundary and interface conditions. In order to have a non trivial solution the determinant of the matrix is set equal to zero leading to an eigenvalue problem to identify ω.

2.4 How to look at the results

To better treat the problem, we use the same adimensionalization as in [5]:

$$Q = \frac{Q_1}{Q_2}, \quad \lambda = \frac{\mu_1}{\mu_2}, \quad Ka = \frac{-\partial_z p R_2^2}{\gamma}, \quad \tilde{k} = kR_1, \quad \tilde{\omega} = \frac{16\omega\mu_2 R_2}{\gamma}.$$

As function of Q, λ and Ka it is possible to uniquely determine the shape of the interface and the velocity at the interface, we can

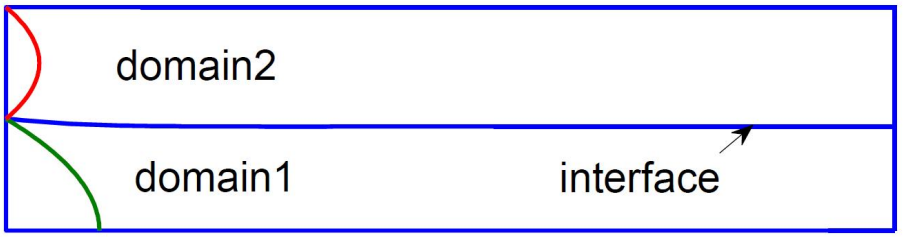

Figure 2.7: Interface position for $Q = 0.7$, $\lambda = 0.5$, $Ka \approx 1$, $R_1 = 0.5$.

thus study the problem in function of the independent dimensionless variable $\tilde{k}$ and dependent variable $\tilde{\omega}$.

From the numerical results in figure 2.8, we can observe that $\tilde{\omega}$ has always the same shape also in different sections, that is also the shape of the analytical form found in [5] in the fully developed region:

$$\tilde{\omega} = \alpha\tilde{k} + iA\left(\left(\frac{\tilde{k}}{b}\right)^2 - \left(\frac{\tilde{k}}{b}\right)^4\right).$$

The difference in our case is that A, b, and α, here constants once Q, λ and Ka are chosen, depend on the axial coordinate at which we perform the analysis,

$$\tilde{\omega}(z) = \alpha(z)\tilde{k} + iA(z)\left(\left(\frac{\tilde{k}}{b(z)}\right)^2 - \left(\frac{\tilde{k}}{b(z)}\right)^4\right).$$

Taking the base flow configuration in figure 2.7, we can see the numerical results for different axial coordinates in figure 2.8. Having noticed this similarity, we follow the same criterion used [5] to understand if the regime is convective or absolutely unstable (cf. fig 2.9), and than if we expect to have jetting or dripping regime. In fact we can find the back velocity v_- and front velocity v_+ of the perturbation imposing

$$v = \frac{\tilde{\omega}_i}{\tilde{k}_i}, \qquad \frac{\partial\tilde{\omega}_i}{\partial\tilde{k}_r} = 0, \qquad v = \frac{\partial\tilde{\omega}_i}{\partial\tilde{k}_i},$$

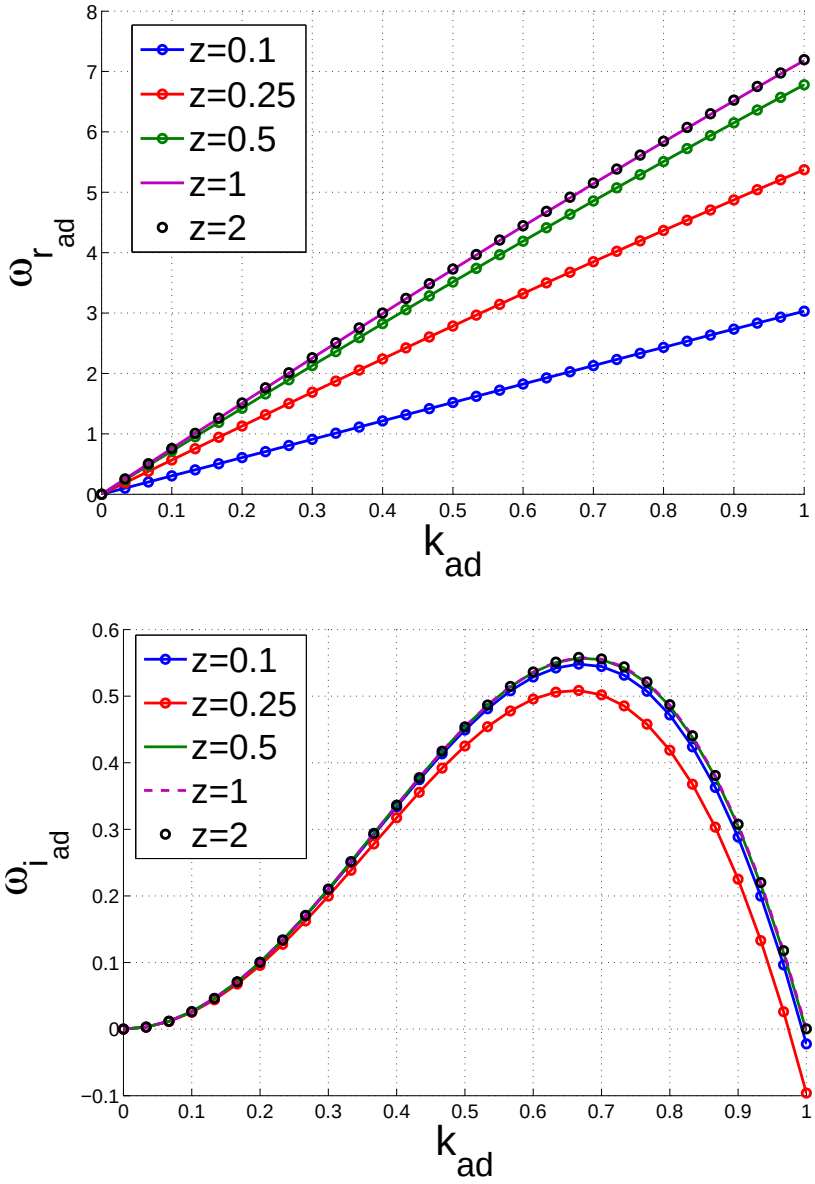

Figure 2.8: Real and imaginary part of $\tilde{\omega}$ for $Q = 0.7$, $\lambda = 0.5$, $Ka \approx 1$, $R_1 = 0.5$.

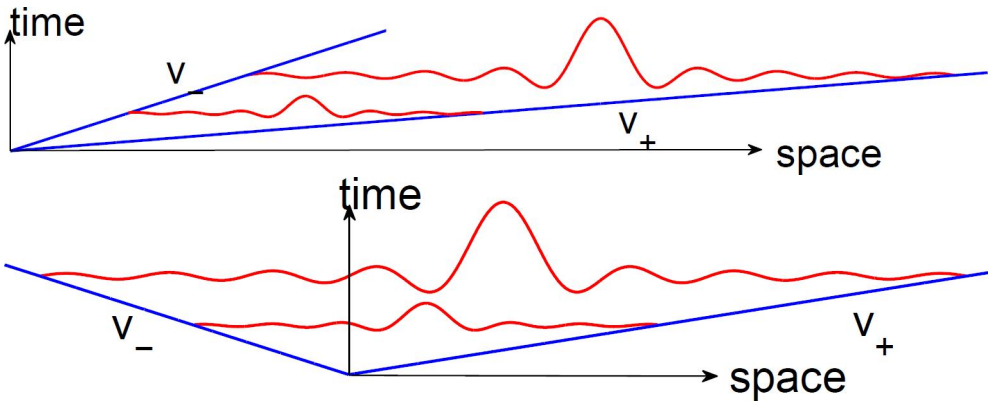

Figure 2.9: Wave packets propagating downstream and upstream respectively.

this criterion leads to

$$v_{\pm} = \alpha(z) \pm A(z)\left(\frac{\sqrt{7}+5}{12b(z)^2} - \frac{\sqrt{7}+5}{36b(z)^4}\right)\sqrt{\frac{24b(z)^2}{\sqrt{7}-1}}.$$

We are interested in the back velocity v_{-}, because if it is positive the wave packet is washed away from the flow, if it's negative the perturbation can go upstream and propagate toward the inlet region leading to dripping regime (figure 2.9). Let's see an example of v_{-} in function of the axial coordinate (figure 2.10) We can observe that close to the inlet we have an absolute regime, this is physically coherent because at the inlet the interface velocity is zero and then the perturbation can easily go upstream.

For this reason we will always expect an absolutely unstable region close to the inlet because the velocity at the interface we will not be high enough to wash the perturbation away. This is why we put another restriction for the instability to be absolute: we say that the length of the absolute region L_{ABS}, has to be long enough to allow the growth of the perturbation. Thus the minimum wavelength of the perturbation λ_{min} must be shorter than the length of the absolute

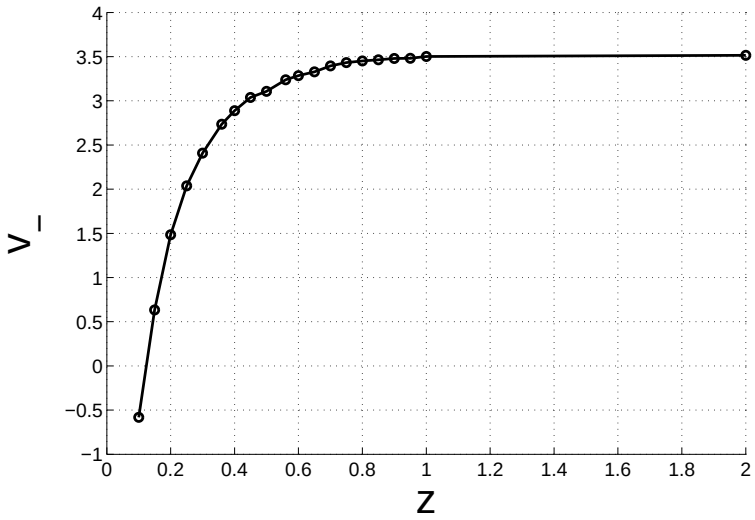

Figure 2.10: Regime of the instability for $Q = 0.7$, $\lambda = 0.5$, $Ka \approx 1$, $R_1 = 0.5$.

region

$$L_{ABS} > \lambda_{min}.$$

We should define λ_{min} with the frequency corresponding to the absolute mode of the perturbation, however we can define in first approximation

$$\lambda_{min} = \frac{2\pi}{k_{cut\ off}}.$$

In the example in figure 2.10 we have $L_{ABS} \approx 0.125$, much shorter that λ_{min}, and in this case, an absolute instability is not expected.

Chapter 3

Results

3.1 Axial dependency of the results

In this chapter we will present the differences in the results of the local stability analysis computed in the region close to the inlet, compared with the results found for the fully developed flow. We also compare the results to the analytical solutions and experimental data presented in [5]. Taking the flow configuration in figure 3.1, we can observe the strong dependence of $\tilde{\omega}$ on the axial coordinate when we have a considerable change of interface position between inlet and fully developed flow. In fact, in this case we have a position of the interface around 0.5 (adimensional unit length) at the outlet and 0.1 at the inlet. Looking at figure 3.2, we notice the different behavior of

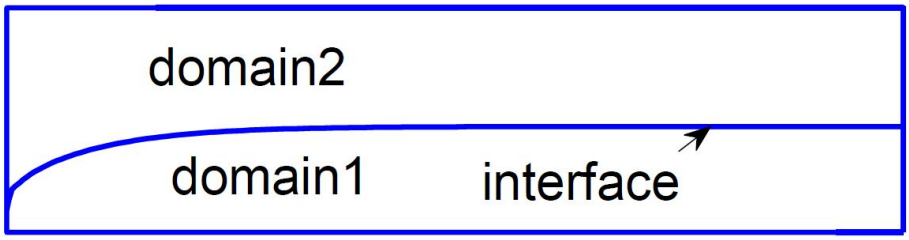

Figure 3.1: Interface position for $Q = 0.7$, $\lambda = 0.5$, $Ka = 1$, $R_1 = 0.1$.

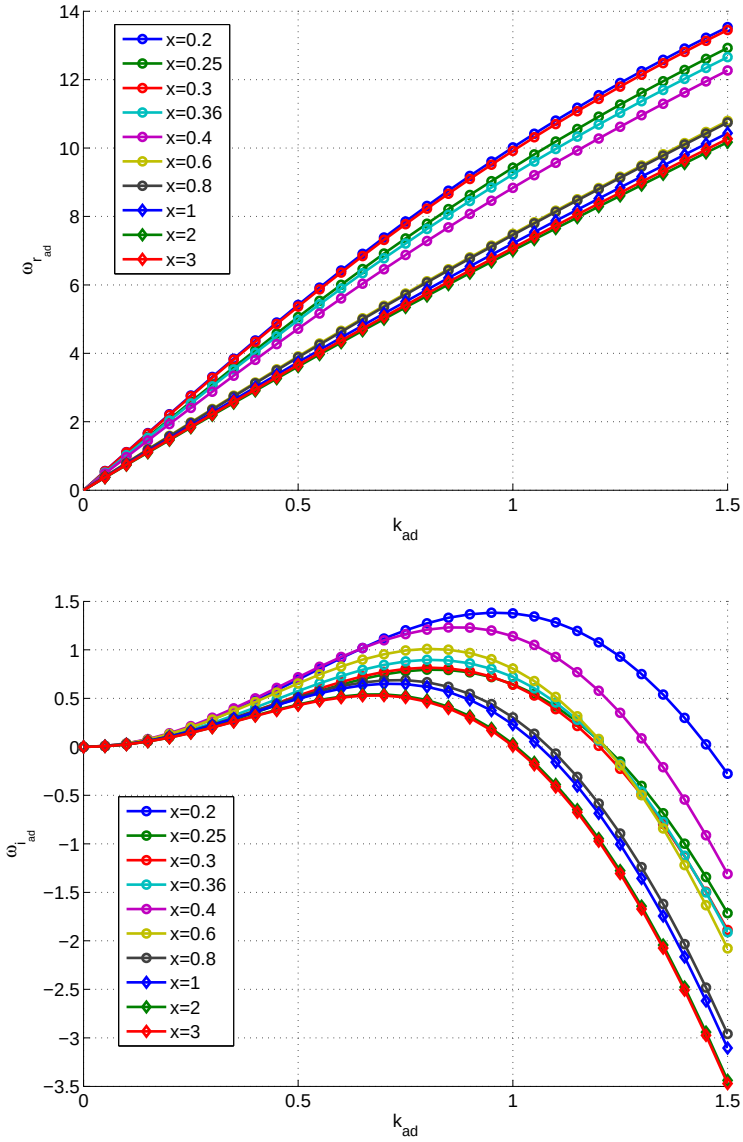

Figure 3.2: Real and imaginary part of $\tilde{\omega}$ for $Q = 0.7$, $\lambda = 0.5$, $Ka = 1$, $R_1 = 0.1$.

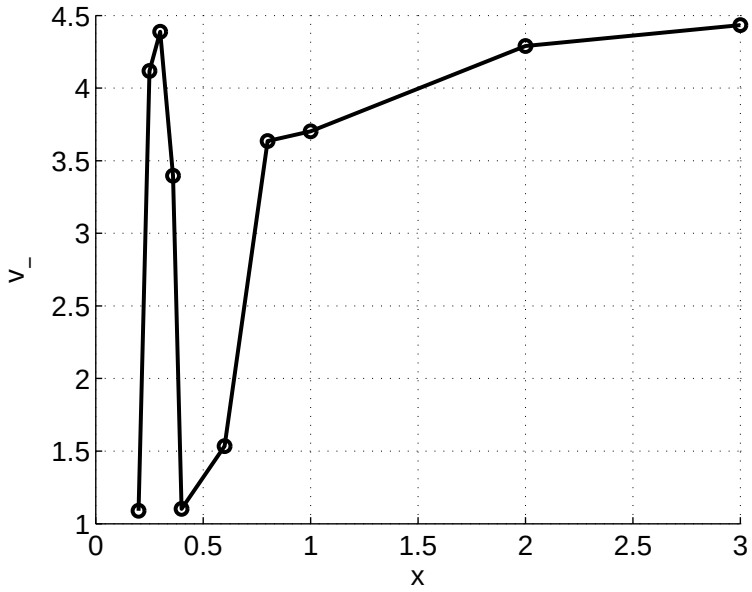

Figure 3.3: Regime of the instability for $\tilde{\omega}$ for $Q = 0.7$, $\lambda = 0.5$, $Ka = 1$, $R_1 = 0.1$.

both real and imaginary part of $\tilde{\omega}$ at different sections. This underlines the fact that it is indeed important to analyze the developing region because it could give quite different results from the region where the flow is fully developed. In figure 3.3 we observe that the regime of the instability is convective everywhere in this case since the velocity of the upstream front of the wave packet is always positive.

3.2 Comparison with previous studies

Here we analyze a case that in the analytic solution proposed in [5] is on the threshold between absolute and convective instability (the configuration is shown in figure 3.4). In figure 3.5 we can see the blue point, that identify the case we analyze, overlapped to the line that

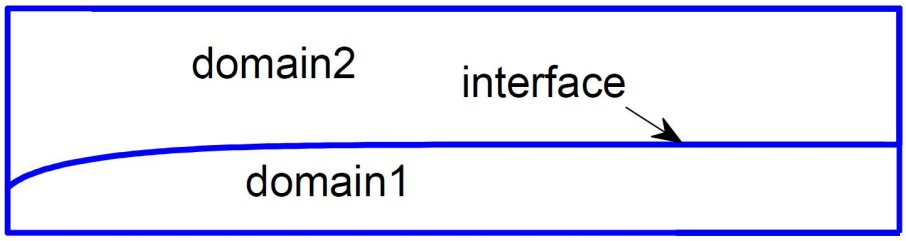

Figure 3.4: Interface position for $Q = 0.5636$, $\lambda = 0.2$, $Ka = 1$, $R_1 = 0.2$.

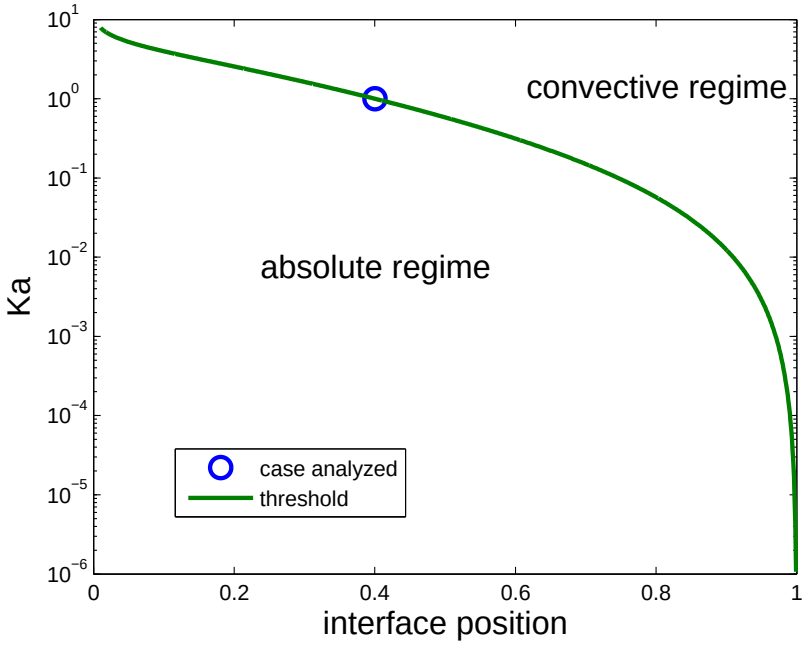

Figure 3.5: Absolute and convective regions in the (x, Ka) plane found analytically in [5].

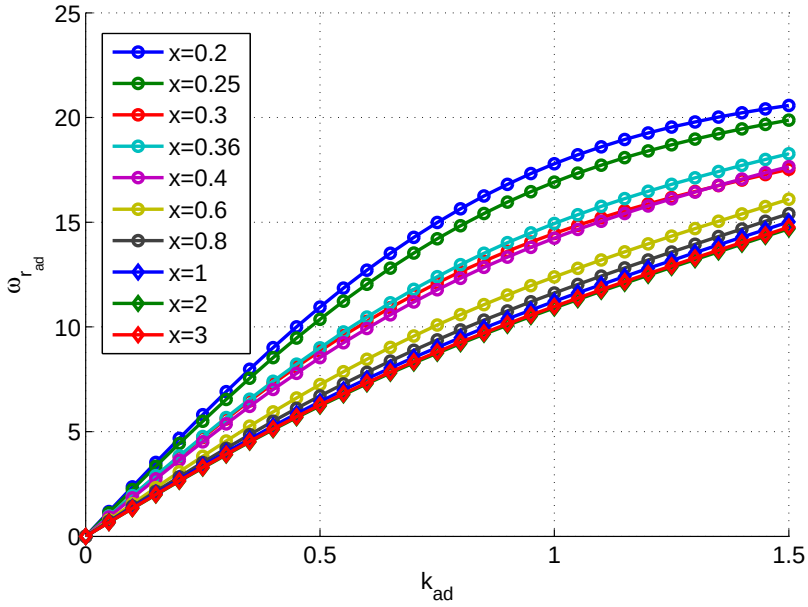

Figure 3.6: Real part of $\tilde{\omega}$ for $Q = 0.5636$, $\lambda = 0.2$, $Ka = 1$, $R_1 = 0.2$.

gives the threshold between absolute and convective region found in [5]. This is a really interesting situation to observe because we can understand if our model gives a more convectively or absolutely unstable solution with respect to the analytical solution cited before.

In figure 3.6 and 3.7 the real and complex part of $\tilde{\omega}$ are shown, and from these the nature of the instability can be inferred (cf. fig. 3.8 where results at different sections z are reported). In figure 3.9 we can see the eigenfunctions corresponding to the maximum value of v_- in the developing region and to the fully developed region. To compare the results shown in 3.8 with the analytical solution we have to look at the fully developed flow, that corresponds to the v_- values on the right of the graph. Here we can notice a clearly convective behavior, and this agrees well with the experimental results in [5], where

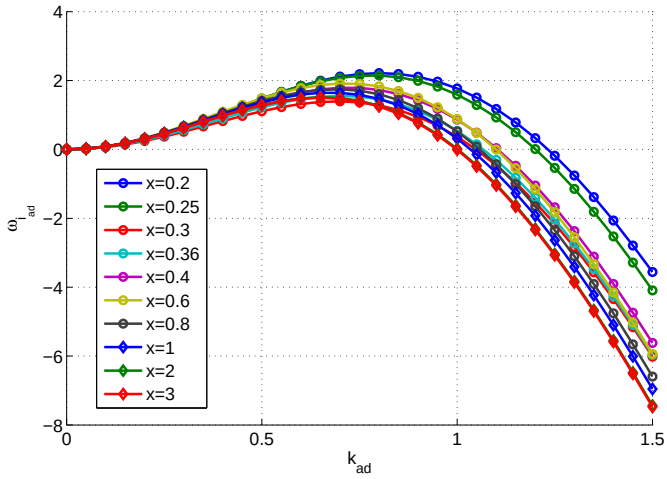

Figure 3.7: Imaginary part of $\tilde{\omega}$ for $Q = 0.5636$, $\lambda = 0.2$, $Ka = 1$, $R_1 = 0.2$.

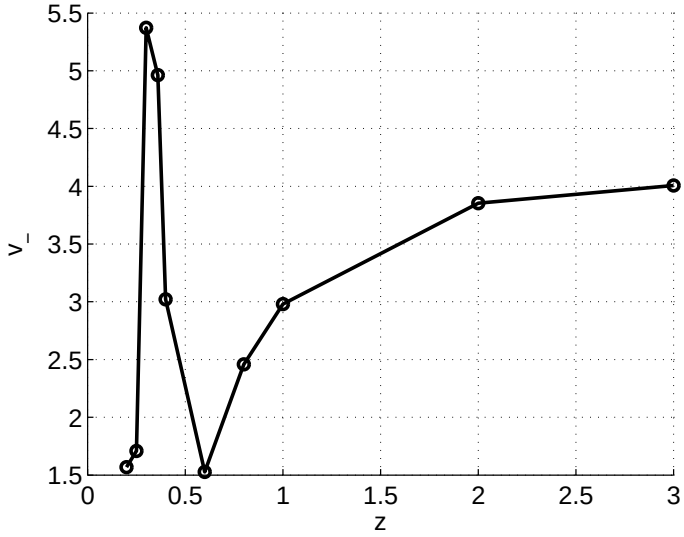

Figure 3.8: Regime of the instability for $\tilde{\omega}$ for $Q = 0.5636$, $\lambda = 0.2$, $Ka = 1$, $R_1 = 0.2$.

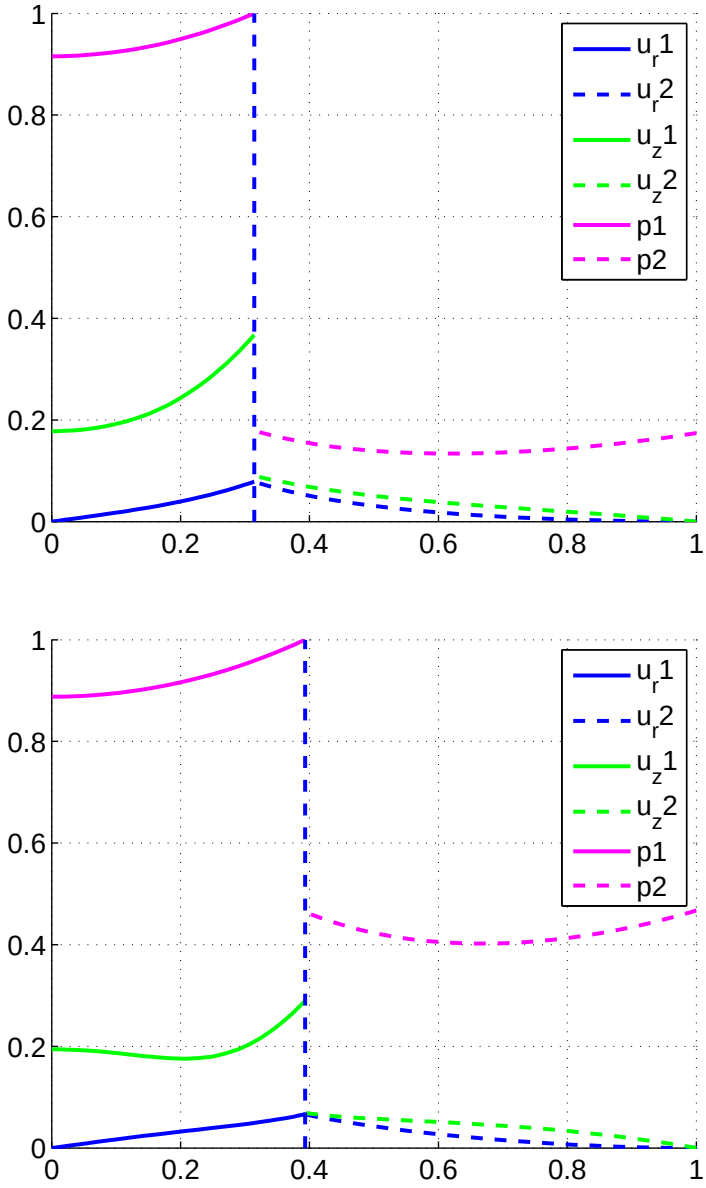

Figure 3.9: Eigenfunctions for $z = 0.3$ and $z = 3.5$.

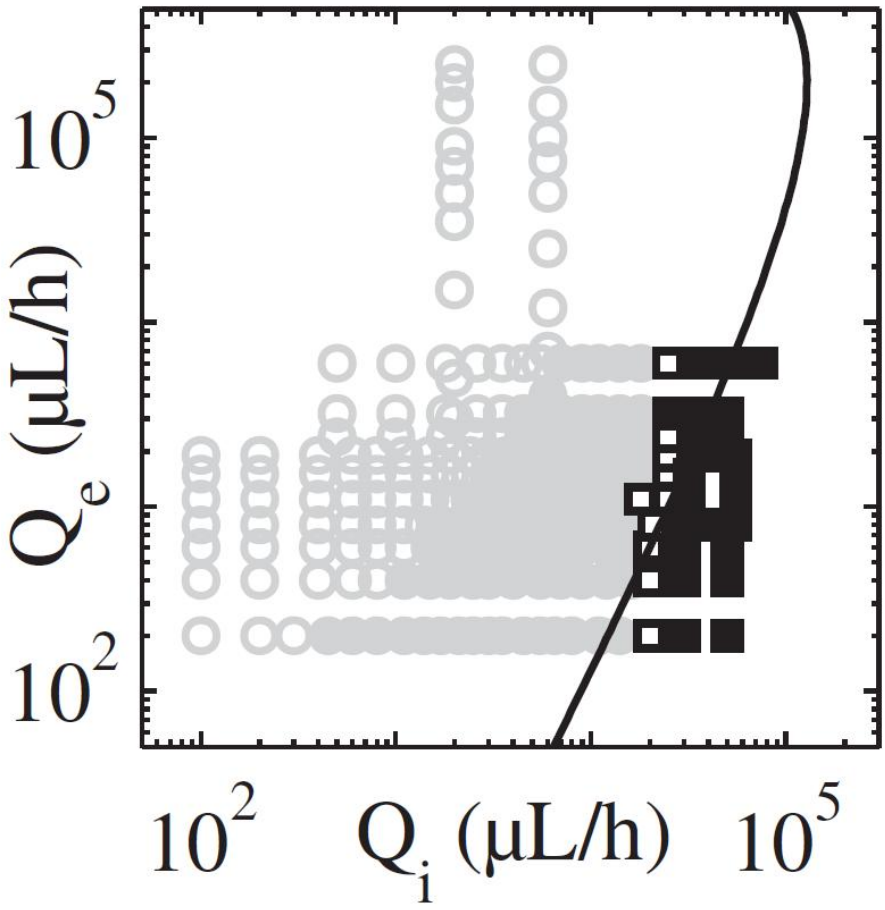

Figure 3.10: Experimental results (gray symbols for dripping, black symbols for jetting) and analytical prediction (absolute to the left of the line, convective to the right of the line) showed in [5] in the plane defined from the inner and outer flow rate (Q_i, Q_e).

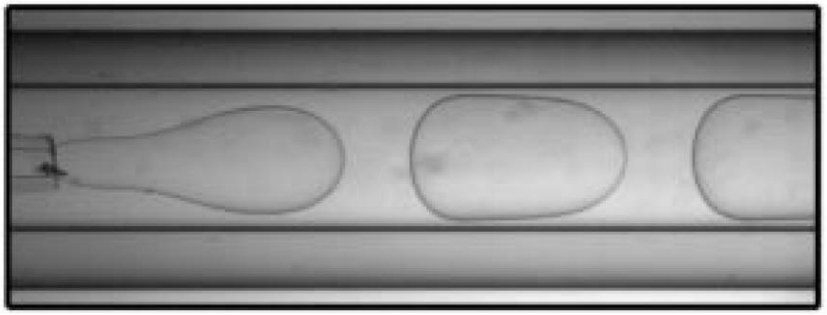

Figure 3.11: Droplets formation in an intermediate regime between dripping and jetting, experimental study presented in [5].

the experimental data give jetting regime (convective), whereas the analytical solution indicates an absolutely unstable behavior. In figure 3.10 we can notice that the differences between experimental data and analytical solutions are significant, considering that a logarithmic scale is used.

It is also of great interest the peak for v_- that we find in the developing region; since this value is higher then the value found for the fully developed region, we could expect a positive v_- even if it is negative in the fully developed region. This particular behavior of v_- (observed both in fig. 3.3 and fig. 3.8) could explain why in some cases the droplets form neither at the inlet nor in the fully developed region, but in the middle (cf. fig. 3.11). It is possible that the disturbance moves upstream from the fully developed region toward the inlet, and this movement would stop when v_- changes sign.

Conclusions and future developments

3.3 Conclusions

The tool developed in this project makes possible to perform local stability analysis on a coaxial jet for different axial coordinates, from the inlet to the fully developed region. What has been observed is the regime (absolute or convective instability) of different flows at different sections in order to determine whenever the system will give rise to droplets formation at the inlet (dripping) or in the fully developed region (jetting).

The study has the purpose to improve our understanding of the results obtained in [5], for the transition between absolute and convective regime. To do that we have focused our attention on values of the parameters governing the problem, for which the flow is close to threshold between absolute and convective regime. Doing this we have been able to have a good comparison between our model, the analytical solutions and the experimental results presented in [5]. The results found are in good agreement with the experimental data; in addition they provide a basis for a better understanding of the phenomena going on in the developing region of the flow.

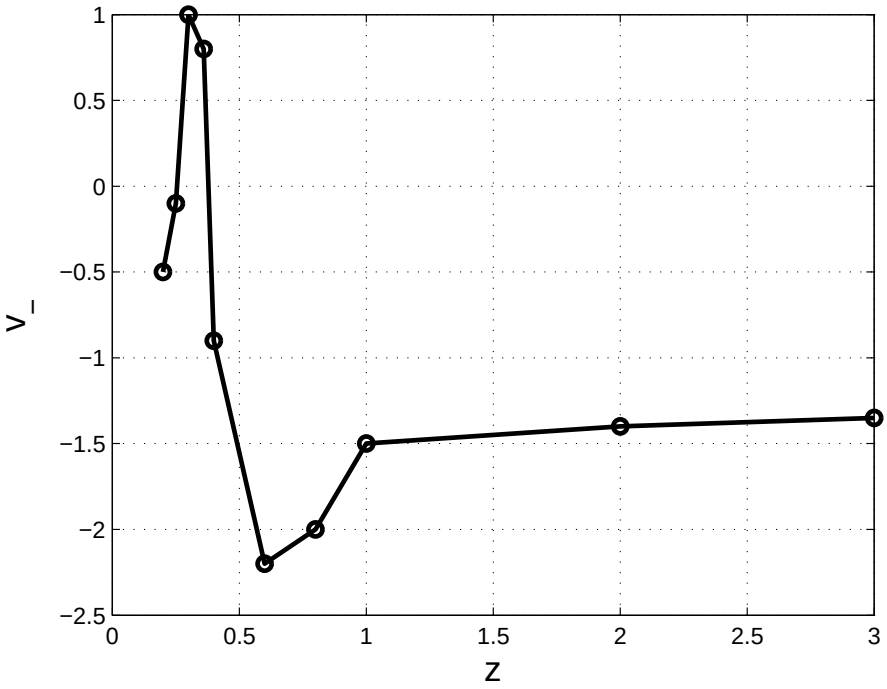

Figure 3.12: Hypothesis on the behavior of the parameter v_- in the case of a mixed absolute and convective regime, v_- determines the absolute (when is negative) or convective (when is positive) regime of the flow.

3.4 Future developments

The first attempt to improve these results would be to find a flow that exhibits a convective regime and absolute regime together, one in developing region and the other in the fully developing region (cf. fig. 3.12). This case would be of great interest in justifying the transition between dripping and jetting.

The following step would be to perform a global stability analysis, in order to take into account the variation of the system in the axial direction. This is probably the best theoretical tool to analyze this phenomenon and remains the main idea to follow in a possible continuation of this project.

Bibliography

[1] Lord Rayleigh, *On the Capillary Phenomena*, Proceedings of the London Mathematical Society, Vol. $XXIX$, pp.71-97 (1879).

[2] Joseph Plateau, *Statique Experimentale et Theorique des Liquides soumis aux Seules Forces Moleculaires*, Gauthier-Villars, Paris, (1873).

[3] Steve Hoats, *Inkjet Printing - the Physics of Manipulating Liquid Jets and Drops*, Journal of Physics 105, 012001 (2008).

[4] Jeong Rim Hwang,Michael V. Sefton, *Effect of capsule diameter on the permeability to horseradish peroxidase of individual HEMA-MMA microcapsules*, Journal of Controlled Release, Volume 49, Issues 2–3, Pages 217-227 (1997).

[5] Pierre Guillot, Annie Colin, Andrew S. Utada, Armand Ajdari, *Stability of a Jet in Confined Pressure-Driven Biphasic Flows at Low Reynolds Numbers*, Physical Review Letters 99, 104502 (2007).

[6] Constantine Pozrikidis, *Boundary Integral and Singularity Methods for Linearized Viscous Flow*, Cambridge University Press (1992).

[7] http://www.freefem.org/